Perovskite-type lanthanum ferrite based photocatalysts: preparation, properties, and applications

Muhammad Humayun[a], Habib Ullah[b], Muhammad Usman[c], Aziz Habibi-Yangjeh[d], Asif Ali Tahir[b], Chundong Wang[a,*], Wei Luo[a,*]

[a]School of Optical and Electronic Information, Wuhan National Laboratory for Optoelectronics, Engineering Research Center for Functional Ceramics of the Ministry of Education, Huazhong University of Science and Technology, Wuhan 430074, PR China

[b]Environment and Sustainability Institute, University of Exeter, Penryn, TR10 9FE Cornwall, United Kingdom

[c]Center of Research Excellence in Nanotechnology, King Fahd University of Petroleum and Minerals (KFUPM), Dhahran 31261, Saudi Arabia

[d]Department of Chemistry, Faculty of Science, University of Mohaghegh Ardabili, P.O. Box 179, Ardabil, Iran

Corresponding Authors Email: apcdwang@hust.edu.cn (C.W); luowei@mail.hust.edu.cn (W. L).

Abstract

Clean energy and a sustainable environment are grand challenges that the world is facing which can be addressed by converting solar energy into transportable and storable fuels (chemical fuel). The main scientific and technological challenges for efficient solar energy conversion, energy storage, and environmental applications are the stability, durability, and performance of low-cost functional materials. Among different nanomaterials, perovskite type $LaFeO_3$ has been extensively investigated as a photocatalyst due to its abundance, high stability, compositional and structural flexibility, high electrocatalytic activity, efficient sunlight absorption, and tunable band gap and band edges. Hence, it is urgent to write a comprehensive review to highlight the trend, challenges, and prospects of $LaFeO_3$ in the field of photocatalytic solar energy conversion and environment purification. This critical review summarizes the history and basic principles of photocatalysis. Further, it review in detail the $LaFeO_3$, applications, shortcomings, and activity enhancement strategies including the design of nanostructures, elemental doping, and heterojunctions construction such as Type-I, Type-II, Z-Type, and uncommon heterojunctions. Besides, the optical and electronic properties, charge carriers separation, electron transport phenomenon and alignment of the band gaps in $LaFeO_3$-based heterostructures are comprehensively discussed.

Keywords: Perovskite-type $LaFeO_3$; solar fuel; photocatalysis; doping; heterostructures.

1. Introduction

In the 21st century, the rapid consumption of fossil fuels by modern society has caused worldwide energy and environmental issues [1]. These are the most serious problems that trouble us physically, economically, and our daily lives. The energy and environmental issues are being linked to some diseases that are around currently. These issues are continuously becoming worse day-by-day [2, 3]. Many factors are present for why the energy and environmental issues become worse around the globe. However, if people of the globe were to tackle these problems, it would absolutely help both the environment and the people live in it [4]. It is expected that the current CO_2 emission in atmosphere as a result of fossil fuel combustion will increase the average temperature of the globe up to 6 ^{o}C till the end of 21st century that will convert the global glacial climate to an ice-free Antarctica [5, 6]. In contrast, the accelerated release of harmful agents by industrial activities has resulted in worldwide air and water pollution which has affected both human beings and the surrounding [7]. Thus, to tackle the energy shortage and the associated environmental tribulations, it is a big challenge for the research communities to search for alternative sustainable and environmentally friendly technologies [8, 9].

Nowadays, solar energy as a sparkling and renewable energy source is used as an alternative to fossil fuels [10]. The consumption of solar energy by semiconductor photocatalysts can produce H_2 through water reduction, convert CO_2 to useful chemicals, and oxidize various pollutants [11, 12]. Thus, semiconductor photocatalysis has been considered clean, economical, renewable, and safe technology [13]. Since the first report on TiO_2 photocatalysis,[14] this field has attracted tremendous attention of scientists all over the world. Numerous semiconductor photocatalysts including ZnO,[15-18]

SnO_2,[19, 20] $BiVO_4$,[21-29] BiOCl,[30] $SrTiO_3$,[31-37] WO_3,[38-42] Fe_2O_3,[43-45] Ta_2O_5,[46-49] $BiFeO_3$,[50-54] Bi_2WO_6,[51, 55-59] Cu_2O,[60-62] g-C_3N_4,[63-67] MoS_2,[68-71] WS_2,[72-74] Graphene,[75-78] Carbon nanotubes,[79, 80] etc. have been extensively employed in photocatalytic solar fuel generation and environment purification.

Many promising environmental techniques for photocatalytic disinfection of water and CO_2 reduction for green and renewable energy have been developed [81-85]. In semiconductor photocatalysis, highly reactive short-lived species are formed on a semiconductor surface under exposure to light energy with wavelength greater or equal to its bandgap [86-88]. The high oxidizing and reducing power of these species can induce pollutant degradation, CO_2 reduction reactions, and water splitting [89-92].

Perovskite-type lanthanum ferrite ($LaFeO_3$) as a visible light active ($E_g = 2.0$ eV) p-type semiconductor has received great attention in scientific research [93]. The general formula used for perovskite-type oxides is ABO_3, where site "A" represents rare-earth ions and site "B" represents transition metal cations [94]. The physical and chemical properties of $LaFeO_3$ are quite distinct from other material that's why it is employed in superior technologies like electromagnetic materials, solid oxides fuel cells, gas sensors, and catalysts [95, 96]. However, the photocatalytic efficiency of $LaFeO_3$ is still insufficient for efficient photocatalysis due to the small surface area of bulk material, limited solar energy consumption, fast charge carriers recombination and positive conduction band (CB) bottom level [97]. The performance of $LaFeO_3$ generally depends on the structure, shape, and size, and the synthesis process will have a great influence on it [98]. Several methods for synthesizing perovskite-type $LaFeO_3$ have been reported, such as the sol-gel, hydrothermal, sonochemical, solvothermal, microwave assisted, and co-precipitation [99]. Among these, only the sol-gel method can produce small and identical $LaFeO_3$ nanoparticles [93]. However, due to its high surface energy, $LaFeO_3$ nanoparticles easily agglomerate, leading to a severe decrease in performance [98]. An effective strategy is to introduce pores in $LaFeO_3$ by various template methods [100, 101].

In addition to the synthesis strategy, the optical absorption of $LaFeO_3$ can be extended by incorporating dopants into its lattice [102, 103]. Based on the estimated valence band (VB) level of $LaFeO_3$ (2.2 V), photo-induced holes possess adequate energy to commence oxidation processes with H_2O/OH^- or could oxidize various pollutant directly [104]. Therefore, it is very important to reduce the inherent band gap of $LaFeO_3$ by elemental doping. The surface states generated by the incorporated dopants will shift the top of its VB upward to a certain extent. As a result, its photocatalytic activity would greatly improve. As reported, the conduction band (CB) level of $LaFeO_3$ is positioned at 0.2 V versus the potential of normal hydrogen electrode (NHE) and is unsuitable for reduction processes. Nevertheless, it can generate high-level energy electrons (HLEEs) above 0 V, which quickly relaxes to the CB bottom and release its potential energy. To utilize these electrons in photocatalytic reduction reactions, it is recommended to design a rational strategy by coupling semiconductors with proper band alignment [105]. Beyond the conventional type-I, type-II, and Z-type heterostructures, uncommon heterojunctions have been developed by some researchers. In such types of heterojunctions, wide bandgap photocatalysts such as TiO_2, ZnO, SnO_2, etc. are coupled with narrow band gap semiconductors like Fe_2O_3, $BiVO_4$, $BiFeO_3$, Bi_2O_3, etc [54, 55, 106-112]. The wide band gap semiconductors operate as proper energy platform for accepting the HLEEs of these narrow bandgap semiconductors. As a result, the HLEEs are utilized in efficient photoreduction reactions in the CB platform of wide band gap semiconductors. Thus, the photocatalytic processes could be made practical by fabricating uncommon heterojunctions. This review aimed to provide a broad overview of the basic principles of photocatalysis, history, applications, shortcomings, activity enhancement strategies, synthesis, doping strategies and heterostructures formation of perovskite-type $LaFeO_3$.

2. Photocatalysis

In this part, our goal is to present a clear description of the photocatalysis. In fact, photocatalysis has been regarded as one of the most advanced technique owing to its outstanding function in environmental clean-up such as self-cleaning of building supplies, anti-bacterial, anti-fogging, and exertion. The photo-catalysis applications are promptly increasing in various fields, and fundamental research work has been widely going at the forefront. In fact, the term "photocatalysis" is inspired by natural photosynthesis. In other words, photocatalysis is the acceleration of photoreactions with the aid of a catalyst. Particularly, the H_2 fuel generation by H_2O splitting with the aid of solar light (so called artificial photosynthesis) is extremely projected as a potential application. Several redox reactions occur on the heterogeneous photocatalysts surfaces via the photo-induced electron-hole pairs. Meanwhile, highly reactive species are produced via the reaction with photo-induced holes and electrons. These reactive species are mainly involved in the oxidative and reductive reactions. The species to which oxygen is highly reactive are called reactive oxygen species (ROS). The ROS mainly comprise superoxide-anion radical ($•O_2^-$), hydroxyl-radical (•OH), hydrogen peroxide (H_2O_2), and singlet O_2 ($^1O_2$), as depicted in **Fig. 1(a)**[113]. These ROS facilitate pollutant oxidation. Besides, the h^+ could directly induce pollutant oxidation or under appropriate circumstances, react with the dissolved O_2 or H_2O/OH. On the other hand, the H^+ and CO_2 are respectively reduced to H_2 and hydrocarbons for favorable energy, while the H_2O/OH^- are transformed to •OH via oxidation reactions[114-116].

2.1 History

In the early 19th century, the Giacomo Ciamician chemist firstly conducted experiments to investigate whether light initiates chemical reactions and performed experiments with blue and red lights [117]. He noticed that the chemical reaction occurred only with the assist of blue light. He carefully ruled out the choice that these reactions were driven by heat produced by light. The term "photocatalysis" firstly come into view in 1911 [118]. In 1924, the bleaching of Prussian-blue caused by ZnO upon exposure to light motivated scientists to utilize ZnO as a photocatalyst for the reduction of Ag^+ to the Ag under solar radiation [119]. Scientists investigated that the already existed photosensitive reactions did not involve light-sensitive catalysts [120]. In 1932, it was reported that the TiO_2 and Nb_2O_5 catalysts could drive the photocatalytically reduction of $AgNO_3$ to Ag and $AuCl_3$ to Au [121]. Subsequently, in 1938, it was investigated that TiO_2 can be used as a photo-sensitizer to bleach dyes in the presence of oxygen [122]. Afterwards, due to the lack of practical applications, interest in photocatalysis became a hobby. In 1973, the conditions changed because of the oil crisis that provoked researchers to search for alternative energy resources to fossil fuels [123]. Besides, the environmental concern due to the large-scale industrial set-up encouraged scientists to search for renewable energy resources [124]. The Bell's team first reported the evolution of O_2 on TiO_2 in 1968 [125]. Later in 1972, Fujishima and Honda reported the photoelectrochemical H_2O oxidation on TiO_2 electrodes under UV-light irradiations [126]. In 1977, researchers reported the photocatalytic H_2O splitting on TiO_2 that yielded H_2 and O_2 (2:1) under argon atmosphere [127]. In 1979, Inoue *et al.* reported the photocatalytic CO_2 reduction using a variety of inorganic semiconductors [128]. Afterwards, researchers devoted time for exploring the basic principles, search of new photocatalytic materials, improving photocatalytic performance and clarifying the reaction mechanisms. In the development of new photocatalytic materials, numerous visible-light and UV-light active semiconductors with high efficiencies than TiO_2 have been investigated [86, 129, 130].

2.2 Basic Principles

According to the first law of photochemistry, the light absorbed by a substance can induce photochemical reactions [131]. Thus, semiconductor photocatalysis is not an exemption to this rule, so photons with high enough energy than the bandgap of a semiconductor must be absorbed to induce a chemical change. This means that if spectrum of the light source does not match the semiconductor electronic structure, then the photons will lose without interacting with the solid material. Thus, choice of the light source seriously influences the energetic competence of the chemical process. Taking into consideration the solar energy as a perfect excitation source for environmental reasons, the search for photocatalysts with appropriate bandgaps is a key worry of research communities working on photocatalysis. Therefore, an optical phenomenon should be considered because it greatly affects the efficiency of photogenerated charge carrier's process, which is the primary step in photocatalysis [132-134].

In terms of reaction mechanisms, semiconductor photocatalysis may be described by three major steps: (i) light absorption and charge carrier's generation, (ii) charge separation, and (iii) initiation of redox reactions at semiconductor surface. The schematic design of semiconductor photocatalysis is provided in **Fig. 1(b)**. When a photocatalyst is irradiated with photon energy equals to or superior to its bandgap, charge carriers are generated, the excited electrons move from the VB to its CB while leaving holes in its VB. (i) The photogenerated electrons and holes transfer to the surface of semiconductor. (ii) Simultaneously, a large percentage of electrons excited to the CB recombine with the VB holes due to electrostatic force of interaction, resulting in reproductive heat. (iii) The electrons in the CB initiate reduction reactions and reduce acceptor species. (iv) On the other side, the VB holes oxidize the surface adsorbed donor species. (v) Because of the existence of surface-active states on semiconductors, surface recombination also occurs [135-138]. Thus, the photo-induced long-lived charge carriers on the surface of semiconductors probably commence various redox processes that mainly depend on the donor and acceptor features of the adsorbed active species.

2.2.1 Principles for H_2O Splitting Reactions

Hydrogen has been considered as a prospective clean and sustainable energy fuel. Since the 1st publication on H_2O splitting by Honda and Fujishima in 1967,[139] the photocatalytic H_2O splitting reactions with the aid of solar light have been extensively used for the generation of H_2 fuel. In order to facilitate H_2O splitting reactions, following points must be considered; (i) The photons energy should be equals to, or superior than the bandgap energies of semiconductors to generate charge carriers; (ii) The CB and VB edge potentials of the photocatalysts should match the H_2O reduction and oxidation potential values such as H^+/H_2 (0 V versus NHE)[130, 140-142] and O_2/H_2O (+1.23 V versus NHE)[26], respectively as illustrated in **Fig. 1(c)**. For H_2O oxidation/reduction reactions, exceptional consideration should be given to the choice of suitable photocatalysts. For example, when a photocatalyst is irradiated under solar light, charge carriers are produced which then transfer to the surface of photocatalyst. The electrons/holes on catalyst surface would reduce/oxidize the adsorbed species to generate H_2 and O_2, respectively, as illustrated in **Fig. 1(d)**. The light absorption and charge migration steps strongly depend on the structural morphology and electronic structure of catalysts. Further, high crystallinity of the photocatalysts has positive effect on their activities, however, the increase in crystallinity decreases the surface defects that acts as the charge carrier's recombination centers. The redox reactions are mainly influenced by the surface active-sites and energy of activation for H_2 and O_2 evolution [130, 143-145]. In order to supply extra activation energy, noble metal nanoparticles as co-catalysts are widely employed.

2.2.2 Principles for CO_2 Conversion Reactions

Due to the rapid utilization of non-renewable fossil energy fuels, the atmospheric CO_2 concentration is increasing day-by-day, and its control is a serious issue for research communities [37, 146, 147]. Mimicking the natural photosynthesis to convert solar energy into chemical-fuels is a forthcoming technology to overcome the energy crisis and greenhouse effect [148-150]. In artificial photosynthesis approach, CO_2 is converted into hydrocarbon fuels via the aid of photocatalysts and solar energy [151-153]. The CO_2 conversion is a complex and multi-electron transfer mechanism that produces various products like, formic acid (HCOOH), carbon monoxide (CO), formaldehyde (HCHO), methanol (CH_3OH), and methane (CH_4). These products are formed at their respective redox potentials vs. the standard hydrogen electrode (SHE) at pH 7 (**see Fig. 1(e)**) [154-157]. In fact, it is difficult to convert CO_2 at room temperature because of its highly stable chemical structure. There are some key factors that influence the CO_2 conversion process. The most important factors include the effective charge separation and band gap alignment of the photocatalysts. The kinetics of the electron transfer to CO_2, the basicity of photocatalyst, and CO_2 adsorption also influence this conversion reaction [158-160].

2.2.3 Principles for Pollutants Oxidation Reactions

Because of the fast growth of human population and industrial development, a variety of toxic pollutants are discharged into the surroundings that not only raised severe environmental issues but also posed a risk to the sustainable growth of human race [111, 161]. The presence of these hazardous pollutants even in low concentration posed serious threats to the living organisms, and their degradation is a big challenge for research communities. Semiconductor photocatalysis is considered as a promising technology to effectively degrade these pollutants into inorganic minerals, without generating secondary pollutants [30, 112, 162-164]. However, the effective degradation of pollutants requires a suitable semiconductor photocatalyst with proper band gap and redox potentials. When a photocatalyst is exposed to light energy equals to, or superior to its energy band gap, charge carriers are generated. The charge carriers will transfer to the surface of photocatalyst and react with the adsorbed O_2, H_2O, and ^-OH species. As widely accepted, the reduction potential value of $O_2/O_2^{\bullet-}$ versus NHE is -0.046 V. On the other hand, the reported oxidation potentials values for $^-OH/{\bullet}OH$ and $H_2O/{\bullet}OH$ are 1.89 and 2.27 V versus the NHE, respectively as illustrated in **Fig. 1(f)** [153, 165-167]. If a semiconductor has proper band gap with its CB and VB potential values suitable for the creation of active species like $O_2^{\bullet-}$ and •OH, then it would probably oxidize various pollutants into inorganic minerals like CO_2 and H_2O.

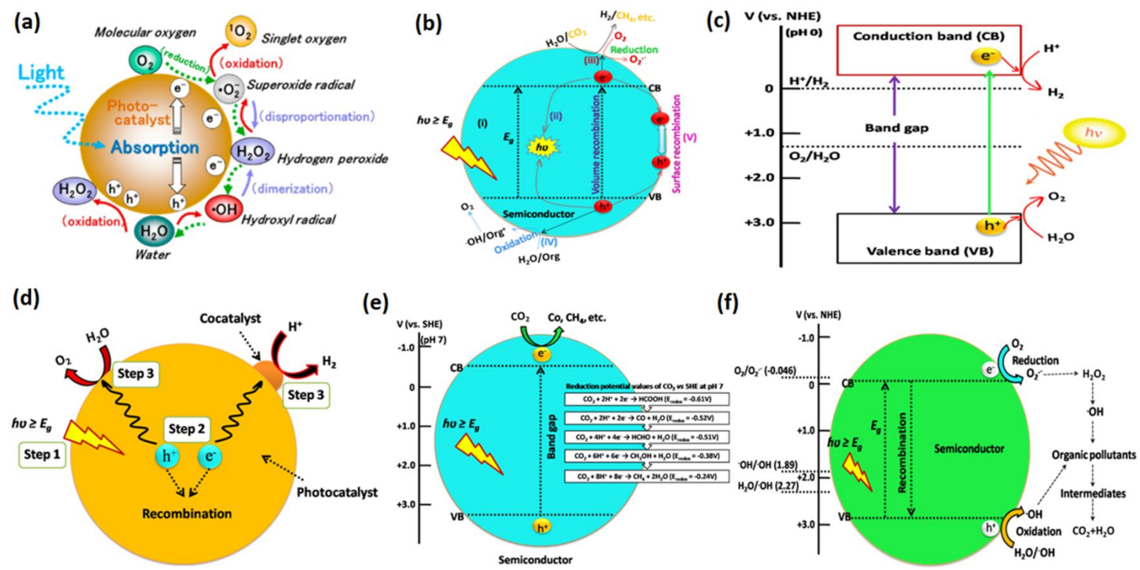

Fig. 1 (a) The ROS produced during photoredox reactions of oxygen and water. Reproduced with permission from ref.[113] Copyright 2017, The American Chemical Society. (b) Proposed schematic for photocatalytic processes. Principles for overall H_2O splitting on semiconductor photocatalyst (c), and the stepwise overall H_2O splitting reactions (d), Adapted with permission from ref. [168] Copyright 2007, The American Chemical Society. (e) Principles of CO_2 conversion over the semiconductor photocatalysts and the reduction potential values versus the SHE at pH = 7. (f) Principles of pollutants oxidation over the semiconductor photocatalysts and oxidation potential values versus the NHE.

3. Perovskite Structures

Materials whose crystal structure resembles calcium titanium oxide ($CaTiO_3$), are called perovskite structures [169]. The perovskite got the name from a mineral discovered by Gustav Rose in the Ural Mountains of Russia in 1839 and finally named after L. A. Perovski ((1792-1856), a Russian mineralogist) [170, 171]. Generally, the structure of an ideal ABO_3-perovskite is cubic with space group of Pm3m [172]. The ABO_3 oxide has

'A' and 'B' site cations of different sizes, which are bonded to the O anion. In ABO_3 perovskites, the 'A' site contains rare earth elements while 'B' site contains 3D transition metals as depicted in **Fig. 2(a)**[173]. The atomic sizes of A-site cations are always larger compared to that of the B-site cations. An ideal cubic structure has six fold coordinated 'B' cations, surrounded by an anion octahedron, and the twelve fold cuboctahedral coordinated 'A' cations. The BO_6 octahedral units share their vertices to form the back bone of the crystal structure, and the site ‘A’ cations occupies the gaps between these units [174-176]. In 1926, the detail investigation on perovskite structure by Victor Goldschmidt led us to the perception of tolerance factor, calculated by taking into account the arrangement of cations and anions radii in the crystal lattice. Generally, the tolerance factor designate the materials stability, purely depending on the ionic size of cations and anions located at the A, B and X sites. The exchange or partial substitution of anions or cations in perovskite structures cause deformation in the cubic structure, leading to the diverse crystallographic arrangement. The perovskites properties mainly depend on the arrangement of atoms of various elements. Many phase transitions take place upon altering the arrangement of atoms that leads to the inspiring selection of optical, electrical and chemical properties. Owing to these flexible tailoring properties, researchers are now paying attention to the perovskite materials due to their diverse applications in optics, sensors, electronics, medicine and optoelectronics. Depending on their capability to occupy various anionic/cationic sites, perovskites exist in diverse structures like oxides, nitrides and sulfides[173, 177]. In this review, we have mainly focused on the oxide of perovskite type lanthanum ferrite.

3.1 Perovskite Type $LaFeO_3$

$LaFeO_3$ orthoferrite belongs to the class of perovskite-type ABO_3 oxides having an orthorhombic structure with Pbnm space groups, which is weakly ferromagnetic [178]. The Fe ions subsystem orders into a moderately tilted anti-ferromagnetic structure with anti-ferromagnetic moment 'G' and weak ferromagnetic moment 'F' [179]. Rare-earth ions gain magnetization 'm' due to interaction with the Fe subsystem [180]. Perovskite-type orthoferrites are mostly interesting because, in contrast to the characteristic scalar product, there is an antisymmetric exchange interaction occupying the vector cross product of adjacent spins. The orthoferrites show anti-ferromagnetic behavior in the absence of this interaction and weak ferromagnetic in its presence. An interesting feature of these materials is that they show a temperature-dependent transformation, in which the direction of the antiferromagnetically ordered spins and the direction of the net magnetization also rotate by 90° [181]. Among different orthoferrites, $LaFeO_3$ received tremendous attention in recent decades owing to its highly stable structure, cheapness, abundance, and proper band gap ~ 2.0 eV [182, 183]. The $LaFeO_3$ structure can be seen as a distorted, corner-sharing network of FeO_6 octahedra, where La cations occupy the gaps between the octahedra as depicted in **Fig. 2(b)**. Unlike the cubic perovskite with a distinct oxygen site, the orthorhombic phase $LaFeO_3$ exhibit two dissimilar oxygen sites, O1 and O2, as depicted in **Fig. 2(c)**. Due to the unique physicochemical properties, $LaFeO_3$ has been utilized in advanced technologies like solid-oxide fuel cells, catalysis, electro-magnetic materials and gas sensors. The physicochemical properties of $LaFeO_3$ mainly depend on its particles size, morphology and structure, which are vigorously influenced by the synthesis progression[93]. In next section, we will discuss about the synthesis routes of $LaFeO_3$.

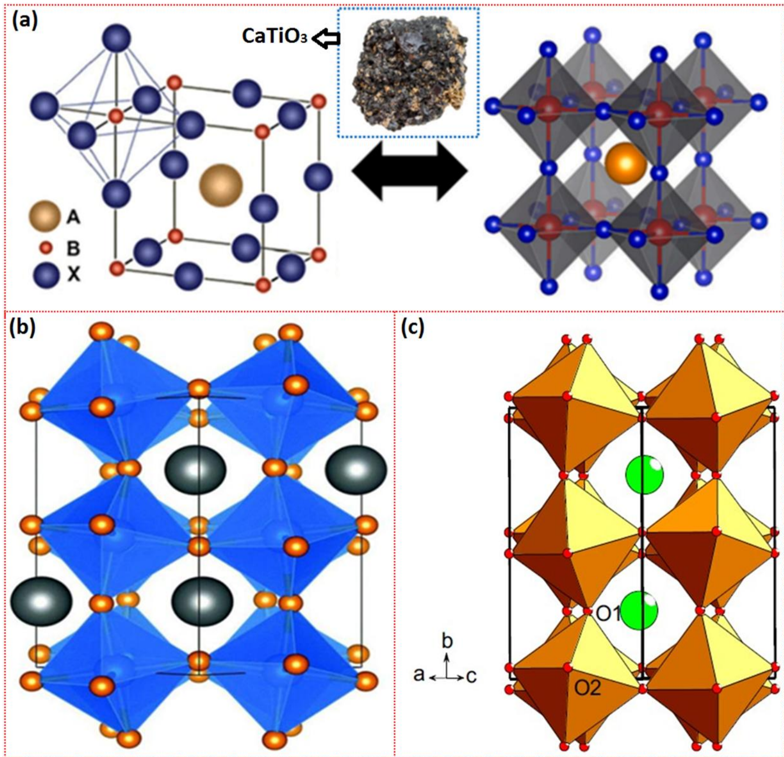

Fig. 2 (a) Perovskites general structure; inset demonstrates the naturally occurring $CaTiO_3$ mineral. Reproduced with permission from ref.[173] Copyright 2021, Elsevier. (b) $LaFeO_3$ perovskite cubic unit cell crystal structure with corner shared FeO_6 octahedrons (blue) and La cations (gray) occupying the interstitial spaces between them. Reproduced with permission from ref.[184] Copyright 2014, The Royal Society of Chemistry. (c) Cubic unit cell with two distinct oxygen sites. Reproduced with permission from ref.[185] Copyright 2015, Elsevier.

4. Synthesis routes of $LaFeO_3$

In fact, a broad variety of synthesis routes exists for the fabrication of $LaFeO_3$ nanostructures and their selection mainly depends on the need and ease of materials availability for various applications. In this section, we will discuss the most frequently used synthesis procedures for energy and environmental applications including hydrothermal, solvothermal, sol-gel, microwave-assisted, and sonochemical.

4.1 Hydrothermal Method

In hydrothermal method, the precursors are heated in an autoclave at elevated temperature and pressure with the aid of H_2O as a solvent. Generally, the employed temperature in hydrothermal process is above 60 °C and below 400 °C that creates high pressure in the closed vessel and assists the solubility of the reactants. Hydrothermal approach is basically a crystallization route including the nucleation and crystal growth as the main steps. Owing to its easy operation, this technique is broadly used for the synthesis of various nanomaterials [186]. This method has a huge effect on the product because only temperature is the controlling parameter. $LaFeO_3$ nanoparticles prepared via hydrothermal route have been widely used in photocatalysis for the purpose of H_2O splitting and pollutant degradation [187-189]. As demonstrated in **Fig. 3(a)**, the $LaFeO_3$ prepared via hydrothermal route exhibited floral-like sheet morphology with high specific surface area of 90.25 $m^2 \cdot g^{-1}$, which resulted in the enhanced visible light degradation of RhB and MB pollutants[190]. Thus, the controlled size and shaped synthesis of nanostructure $LaFeO_3$ via hydrothermal route is a promising research area in the nanoscience and nanotechnology.

4.2 Solvothermal Method

The solvothermal approach is similar to hydrothermal one, but the only difference is that a variety of non-aqueous solvents are used in this method. This method mainly depends on factors such as temperature, pressure, and solvent. In the solvothermal process, the rise in temperature directly influences the synthesis by remarkably decreasing the size of nanoparticles [191]. Kominami *et al.*[192] prepared $LaFeO_3$ nanoparticles via solvothermal decomposition of lanthanum(III)-isopropoxide and iron(III)-butoxide mixture in toluene solvent. In order to achieve nanoparticles with controllable size and morphology, surfactants are frequently added during the reaction. During post treatment of solvothermal technique, the polar or non-polar solvents (ethanol/hexane) could be used for washing the oxide/fluorides, whereas, the non-polar solvents like toluene or hexane could be used for washing the chlorides and bromides.

4.3 Sol-gel Method

Sol-gel technique is the commonly used method that produces highly pure nanomaterials by room temperature treatment. This method assumes colloidal with the solution and gel formation. Generally, metal alkoxides are employed as precursor materials that serve as monomers for polymerization followed by hydrolysis, condensation, and crosslinking to produce a gel. Sol-gel is an extensively used method for the preparation of ceramics and large surface area nanomaterials [193]. The sol-gel technique mainly depends on pH and temperature. There are abundant reports on the synthesis of $LaFeO_3$ by sol-gel technique [194-197]. Tijare *et al.*[182] reported the fabrication of $LaFeO_3$ nanoparticles via a sol-gel route that showed superior activity for H_2 production under visible light irradiations with the aid of co-catalyst Pt. The $LaFeO_3$ prepared via sol-gel method also exhibited high performance for water decomposition [198]. Rao *et al.*[199] fabricated $LaFeO_3$ nanoparticles via sol-gel process. **Fig. 3(b)** reveals that $LaFeO_3$ has irregularly patterns of spheres with dimension of 20 nm. The HRTEM micrograph (**Fig. 3(c)**) reveals lattice fringes with d-spacing of 0.27 nm, corresponding to the (121) plane of orthorhombic phase. The multi-diffraction rings (**Fig. 3(d)**) reveals polycrystalline nature. The particles showed enhanced activity for diclofenac degradation. This technique has advantage over others, because it is used for preparation of $LaFeO_3$ with superior phase-formation temperatures.

4.4 Microwave-assisted Method

In this technique, microwave radiations are used for heating the reaction mixture, and nanomaterials are obtained. The accomplishment of elevated temperature and pressure by the microwave treatment improves the homogeneous mixing and rate of reaction [200]. Farhadi *et al.*[201] reported large surface area $LaFeO_3$ nanoparticles synthesized via a microwave-assisted method. In another report,[202] $LaFeO_3$ nanoparticles prepared via microwave-assisted method, which showed superior photocatalytic performance for methylene blue degradation. This method also made a considerable contribution in combination with other synthesis routes like hydrothermal, sol-gel, etc. For example, Kostyukhin *et al.*[203] reported the synthesis of highly crystalline $LaFeO_3$ via a one-step hydrothermal microwave-assisted technique. As shown in **Fig. 3(e)**, $LaFeO_3$ obtained via a combined microwave-assisted sol-gel method showed enhanced photoactivity for methylene blue decolorization [204]. The microwave assisted technique come into view as a new synthesis method and greatly explored in the terms of organic/inorganic synthesis owing to the diverse benefits like quick reaction time, homogeneous micro-waving, along with the green and proficient energy purpose[205]. Thus, these abundant features make it a suitable procedure for $LaFeO_3$ synthesis.

4.5 Sonochemical Method

This method involves an indirect contact between the metal oxides precursor and ultrasound wave via acoustic cavitation. The ultrasound wave produces bubbles in the reaction cell that oscillates with collecting ultrasonic-energy and grows in size. The extreme growth in size eventually leads to its implosive collapsing and releases the stored energy that enhances the development of nanomaterials. This is an ideal method because reactions occur at ambient temperature and pH is the key factor that influences the nanomaterials formation [206]. Mehdizadeh *et al.*[207] reported the fabrication of $LaFeO_3$ via a sonochemical process that exhibited enhanced activity for pollutant degradation. The key advantage of this technique is achieving nanometric size fine particles of $LaFeO_3$.

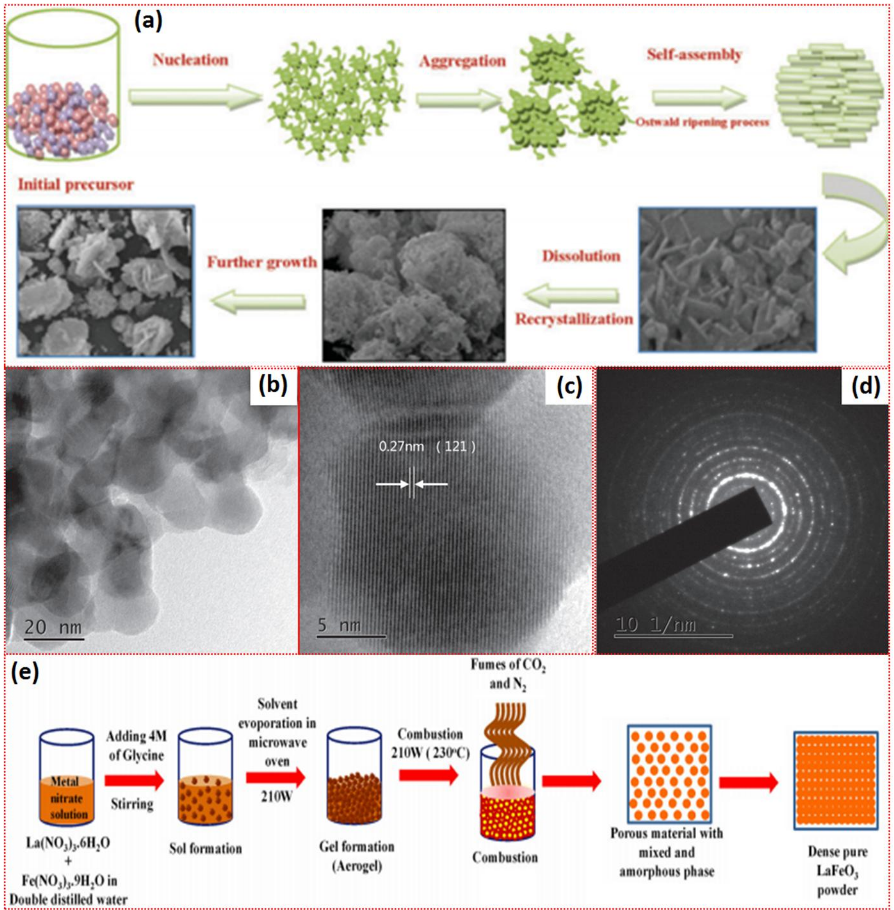

Fig. 3 (a) Schematic of the synthesis of floral-like nanostructure $LaFeO_3$ comprised of sheets. Reproduced with permission from ref.[190] Copyright 2014, The Royal Chemical Society. (b) TEM image; (c) HR-TEM image; and (d) SAED patterns image of $LaFeO_3$ obtained via sol-gel technique. Reproduced with permission from ref.[199] Copyright 2018, Elsevier. (e) Schematic of the $LaFeO_3$ prepared via the microwave-assisted sol–gel route. Reproduced with permission from ref.[204] Copyright 2015, Springer Nature.

5. Applications and Shortcomings

$LaFeO_3$ has broad applications in photocatalysis, gas sensing, electrocatalysis, chemical sensing, electronic materials, magnetic materials, superconductors and solid oxide fuel cells as depicted in **Fig. 4**. The crystal structure of $LaFeO_3$ has corner associated BO_6 octahedral units and twelve coordinated A-site oxygen cations, placed in between the eight BO_6 octahedral units, thereby resulting in a cubic lattice structure, as shown in **Fig. 2(b)**. Depending on the ionic radii and electro-negativity of A-site and B-site cations, orientation of octahedral units takes place, giving rise to lower symmetry structures. The B-site cations have strong interaction with the oxygen anions, while, the A-site cations have comparatively weak interaction with oxygen. Depending on the cation types that occupy the crystal lattice sites, these interactions could be changed to produce various crystal geometries. Thus, diverse tilting degrees of the octahedral units give rise to various crystal fields, resulting in special optical and electronic properties[208]. This might either influence the band structure, photoluminescence, dielectric, and electron-hole transportation behavior of $LaFeO_3$. Hence, due to the distinctive crystal structure, high stability, non-toxicity, and cheapness, $LaFeO_3$ has been regarded as a potential candidate in photocatalysis. It is potentially better than other oxide photocatalysts, owing to the comparative electronic properties such as electrons mobility, charge carriers separation, and photo-induced lifetimes, etc [190, 209]. Regrettably, $LaFeO_3$ still exhibits weak photocatalytic performance due to the existing problems as mentioned below; (i) Large particles size and small surface area; (ii) Weak crystallinity due to low temperature treatment; (iii) Low O_2 adsorption; (iv) Low surface photocatalytic reactions. (v) Limited visible light response and (vi) Fast charge recombination rate. Thus, in section 6, we will highlight the modification strategies for improvement of the overall photo-redox properties of $LaFeO_3$ via various means. This review emphasizes the photocatalytic reaction mechanism and the design of $LaFeO_3$ nanomaterials in detail.

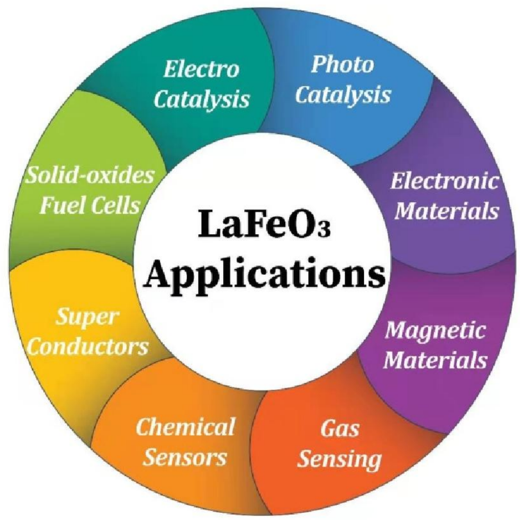

Fig. 4 Schematic for various applications of perovskite-type $LaFeO_3$ material.

6. Modification strategies

The existing problems could be solved by various modification strategies as mentioned below; (i) The small surface area and large particle size problems could be solved by synthesizing controllable sized porous nanoparticles via template assisted methods. As we know, catalysis belongs to the class of surface reactions. Hence, the pores will provide more active sites and promote the transportation of substances. This will enhance the chances of photocatalytic reactions leading to the greatly improved photocatalytic activities; (ii) The crystallinity of nanoparticles mainly depends on the conditions of temperature and reaction time. In order to improve the degree of crystallization and size control, we need to control the reaction time, and subsequently the reaction temperature;

(iii) By introducing co-catalysts, the reactions between electrons and O_2, holes and water could be promoted; (iv) Most probably, the limited optical absorption response of $LaFeO_3$ could be solved by reducing its energy band gap via metal and non-metal doping. This will create new energy states for capturing electrons and holes. As a result, the visible light absorption will enhance leading to the promoted photocatalytic performance; (v) The charge carrier's separation could be promoted via coupling other semiconductors with proper energy band gaps. The schematic for modification strategies is depicted in **Fig. 5**. It has been demonstrated that due to the more positive CB bottom energy level of $LaFeO_3$, photo-induced electrons exhibit insufficient energy to initiate reduction processes. However, upon exposure to visible light, it can generate high-level energy electrons (HLEEs), which can be utilized for effective photocatalysis. It is clear that the HLEEs excited from the VB of narrow bandgap semiconductors upon exposure to visible light could move thermodynamically to the CB of wide bandgap semiconductors such as TiO_2, and ZnO in the composites [104, 105]. This will prolong the lifetime of photo-induced highly energetic electrons, which can be utilized for efficient photocatalysis.

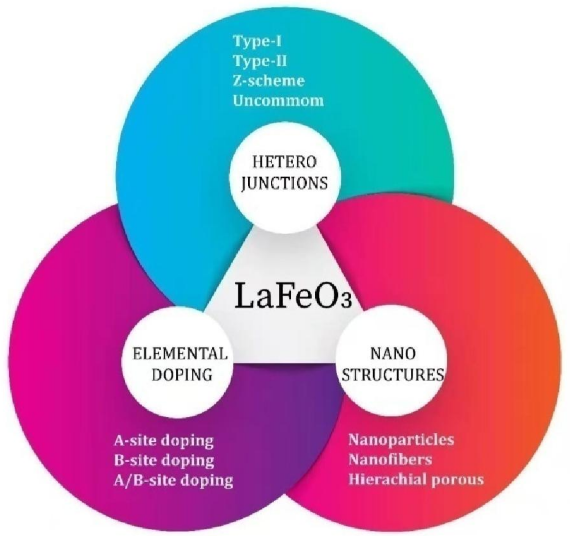

Fig. 5 Schematic for various modification strategies of perovskite-type $LaFeO_3$ catalyst.

6.1 Doping Strategy

The doping history can be traced back to 19th century. In 1930,[210] Gudden observed that the conductivity of a semiconductor is because of the presence of a small quantity of impurity. In 1931,[211] Wilson applied the quantum mechanical conformity to semiconductors. Later on, some pioneering works on rectifiers put forward the idea of *p*-type and *n*-type doping [212]. In 1938, Davydov reported the first model of *p–n* junction and explained the significance of minority carriers [213]. The concept of "doping" first came into view in 1944,[214] when Woodyard experimentally developed a nonlinear circuit-device utilizing germanium (Ge). He incorporated minute controlled quantities of phosphorus (P), antimony (Sb), and arsenic (As) into "Ge" to enhance the electrical conductivity of the circuit-junctions. Later on, Shockley theoretically presented the foremost innovation named "junction transistor" in 1949. He postulated that the new device is advanced to that of the point contact-type device [215]. Nevertheless, the construction of junction-transistors was troubled by a serious issue i.e. the device need a thin-spaced back-to-back joined interlayer of two *p–n* junctions [216]. This problem was solved in 1950 by Spark and Teal, while working in Bell's team and constructed a grown junction transistor by double doping technique. In first step, they transformed the molten form of *n*-type Ge into *p*-type via the addition of a minute quantity of pure gallium (Ga). In second step, they transformed the *p*-type Ge back to *n*-type via the addition of a minute quantity of Sb [217]. Consequently, two different kinds of dopants were simultaneously incorporated in Ge. Thus, the *p–n* junction can be viewed as co-doping *p*-type and *n*-type dopants into semiconductors at dissimilar locations. The most common strategy for improving the efficiency of semiconductor photocatalyts is to dope impurity so as to increase the photon capture efficiency in visible light region. Normally, doping creates intra band gap energy levels that absorb visible light and utilizes a wide range of solar spectrum in photocatalysis as shown in **Fig. 6(a)**. Elemental doping in perovskite oxides typically affects their tunable band gaps and luminescence properties. Normally, A- and B-site doping in perovskite oxides slightly increases or decreases the band gaps depending on the size of the incorporated cations. In general, large size dopants will decrease their band gaps, while small size dopants will increase their band gaps. This is mainly due to the altering of bond lengths and bond angles [218]. Maity et al. [219] demonstrated that Pr doping remarkably decreased the band gap of $LaFeO_3$ by generating new electronic states, and drastically improved the photocatalytic performance for RhB degradation due to the increased light absorption and enhanced charge separation. A similar trend was found in the case of rare earth metal cations like Eu^{3+}, Gd^{3+}, Dy^{3+}, and Nd^{3+} doped $LaFeO_3$ [220]. This fashion could be clarified based on doping site preference. Several reports highlighted the effect of dopant types on the catalytic activity. For instance, Zhong et al.[221] confirmed that the catalytic activity of ABO_3 perovskites is mainly associated with B site metal ions. For the rare earth metal cations like Eu^{3+}, Gd^{3+}, Dy^{3+}, and Nd^{3+} doped perovskite oxides,[220] the ionic-radii of these metal-ions are quite larger compared to the ionic radii of Fe^{3+} cation, as a result, they occupy B sites. Hence, incorporation of these metal ions in $LaFeO_3$ resulted in the crystal lattice distortion that leads to various defects and improved the absorption of dye molecules. The photocatalytic performance for dye degradation was attributed to the combined effect of lattice distortion, surface-exposed active sites, surface defects, and a decrease in the crystallite size of $LaFeO_3$ as a result of the doped metal ions. Similarly, other reports [222-224] about incorporation of Cu^{2+} in $LaFeO_3$ resulted in the improved light absorption and photocatalytic activity for pollutants degradation. Beside, metal doping, non-metal doping can also enhance the optical absorption behavior of $LaFeO_3$ that leads to the enhanced visible-light activities. For instance, Wu et al.[102] reported boron-doped $LaFeO_3$ photocatalysts that revealed enhanced activities for phenol degradation under visible light irradiations. The XRD patterns (**Fig. 6(b)**) of the photocatalysts exhibited high crystallinity and were indexed to the orthorhombic phase, which is highly favorable for photo-induced electron-hole pair's separation and activity enhancement. As can be seen from **Fig. 6(c)** inset, the optical absorption characteristics were remarkably changed with increasing the boron content. The TEM micrograph of boron-doped $LaFeO_3$

photocatalyst (**Fig. 6(c)**) revealed a hexagonal shape and the HRTEM micrograph (**Fig. 6(d)**) clarified the interplanar (101) spacing of 0.38 nm. The photocatalytic activity for phenol degradation was drastically improved as revealed in **Fig. 6(e)**, and a schematic reaction was proposed as shown in **Fig. 6(f)**. Thus, it is concluded that elemental doping in $LaFeO_3$ could play a vital role in enhancing the light absorption, thereby optimizing the photocatalytic performance.

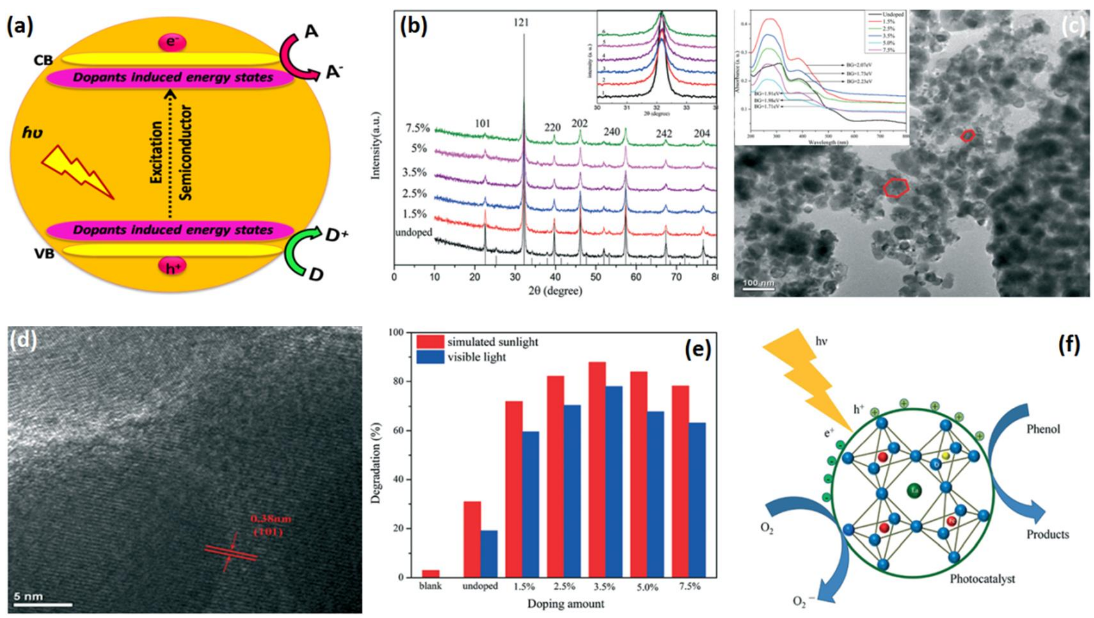

Fig. 6 (a) Schematic illustration of doping induced intra-band gap energy levels in a semiconductor. (b) XRD patterns of pure and boron doped LaFeO3. (c) TEM image of boron doped $LaFeO_3$ with inset UV-vis absorption spectra of the samples. (d) HRTEM image of boron doped $LaFeO_3$. (e) Photocatalytic activity for phenol degradation under simulated and visible light. (f) Schematic for photocatalytic reaction route. Reproduced with permission from ref.[102] Copyright 2015, The Royal Society of Chemistry.

Some typical examples of the dopants incorporated $LaFeO_3$ photocatalysts and their activities are provided in Table 1.

Table 1 Some typical examples of the dopants incorporated $LaFeO_3$ photocatalysts.

Doped $LaFeO_3$ photocatalysts	**Photocatalytic reactions**	**Reference (Year)**
Cu-doped $LaFeO_3$	Methyl orange (MO) degradation	[223](2018)
Li-doped $LaFeO_3$	Methyl blue (MB) degradation	[225](2006)
Ru-doped $LaFeO_3$	H_2 evolution	[226](2017)
Pr-doped $LaFeO_3$	Rhodamine B (RhB) degradation	[219](2019)
Ca-doped $LaFeO_3$	MB degradation	[227](2010)
Ti-doped $LaFeO_3$	Photocatalytic H_2O treatment	[228](2020)
$Eu^{3+,}$ Gd^{3+}, Dy^{3+}, Nd^{3+} doped $LaFeO_3$	SO and RBY dyes degradation	[220](2019)
Sr-doped $LaFeO_3$	2,4-dichlorophenoxyacetic acid	[229](2020)
Ti-doped $LaFeO_3$	Photocatalytic H_2O treatment	[230](2019)
Ba, Ca, Sr, Mg, Fe doped $LaFeO_3$	Congo red (CR) dye degradation	[231](2020)
Zn-doped $LaFeO_3$	MB degradation	[232](2009)
Cu-doped $LaFeO_3$	Bisphenol A degradation	[224](2020)
Ti-doped $LaFeO_3$	Photocatalytic H_2O treatment	[233](2020)
Cu-doped $LaFeO_3$	Atrazine degradation	[222](2019)
B-doped $LaFeO_3$	Phenol degradation	[102](2015)

6.2 Heterojunctions Construction

The design of $LaFeO_3$-based heterostructures is engineered by utilizing both of the $LaFeO_3$ and the coupled semiconductor components under solar irradiations. In $LaFeO_3$ heterostructures, the VB and CB positions of some distinctive semiconductors versus SHE at pH=7.0 are described in **Fig. 7** [234].

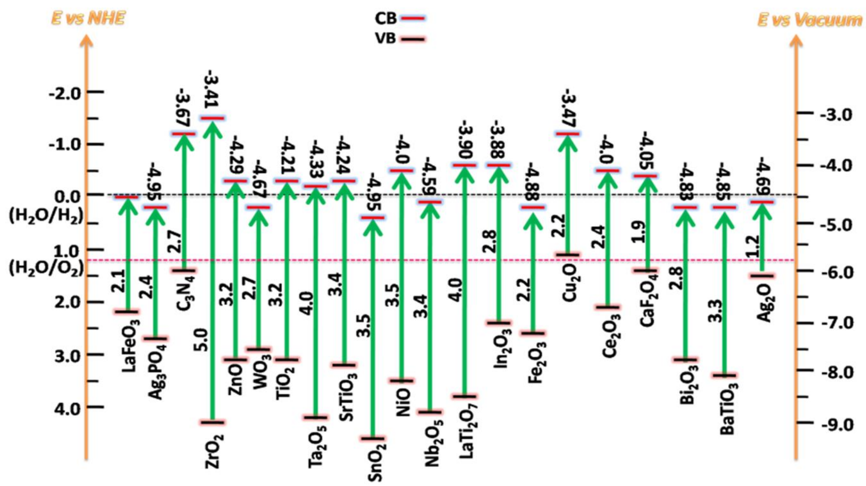

Fig. 7 Schematic of the energy bandgap energies and the VB and CB positions of several distinctive semiconductors versus NHE at pH=7. Reproduced with permission from ref [199] Copyright 2018, Elsevier.

As $LaFeO_3$ is coupled with semiconductors having diverse electronic and band structures, innovative electronic structural configuration are produced due to band bending, that originate potential differences in the hetero-junction areas. At once, an interfacial built-in electric field is created, which promote charge carrier separation and migration. Based on the VB and CB potential values, the $LaFeO_3$ based heterojunctions can be categorized into four main kinds such as Type-I, Type-II, Z-scheme, and uncommon heterojunctions as depicted in **Fig. 8**. In Type-I system, the CB level of the semiconductor 1 locates above the CB level of the semiconductor 2, while the VB edge of the semiconductor 2 locate above the VB edge of the semiconductor 1. Thus, the charge carriers would migrate from semiconductor 1 to semiconductor 2. In such systems, usually the redox activities are very weak[114]. In Type-II heterojunctions, band gaps of the two coupled semiconductors form a staggered alignment, because the conduction and valence band potentials of one semiconductor are reasonably higher than the second semiconductor. As a result, following the early production of electron-hole pairs under the external stimulus, the charge carriers have a tendency to transfer towards opposite directions through interface, leading to spatial separation and subsequent built-in the electric-field[235]. A direct Z-scheme composite represents a feasible strategy for improving the photo-activity. Particularly, the direct Z-scheme structure is similar to the Type-II one, but its charge carriers transport mechanism is different. In a typical direct Z-scheme system, the charge carriers transfer pathway resembles the letter "Z". In other words, due to the low reduction ability of the photo-excited electrons of semiconductor 2, they will recombine with the photo-excited holes of semiconductor 1, which has weak oxidation ability. Thus, the excited electrons in semiconductor 1 with high reduction ability, and the holes in VB of semiconductor 2 with high oxidation ability can be maintained. In this system, the redox ability of catalyst could be optimized[236]. In uncommon systems, the visible light excited high level energy electrons of narrow band gap semiconductors would transfer to highly negative CB of wide band gap semiconductors for reduction processes. Meanwhile, the VB holes of narrow band gap semiconductors would contribute to oxidation reactions[104]. In $LaFeO_3$-based heterojunctions, $LaFeO_3$ might be used as semiconductor number 1 or 2, depending on the band edges of the coupled semiconductors. In $LaFeO_3$-based type-I heterojunction (**Fig. 8(a)**), the CB of $LaFeO_3$ should be more negative and its VB should be positive compared to the CB and VB of the coupled semiconductors. Hence, the photo-induced electrons and holes of $LaFeO_3$ would migrate to the CB and VB of the coupled photocatalysts for redox reactions, respectively. In $LaFeO_3$-based Type-II heterostructures (**Fig. 8(b)**), the CB potential of semiconductor-1 should be more negative compared to the CB of semiconductor-2. Likewise, its VB edge should be less positive than the VB edge of semiconductor-2. Hence, under solar irradiations, band bending is produced at interfacial junction, and the electron and holes move in opposite directions. Type-II heterojunction is more beneficial due to the highly efficient charge carriers separation. In addition, the surface redox reactions occur in two different semiconductors. In Z-type heterostructures (**Fig. 8(c)**), the photo-induced electrons of the semiconductor-2 with less negative CB edge would combine with the holes of semiconductor-1 having less positive VB edge, leaving behind electrons in the highly negative edge CB of semiconductor-1 and holes in the highly positive VB edge of semiconductor-2. Thus, the wonderful Z-scheme heterojunction displays a dual function in catalysis such as better charge carriers separation and also strong reduction/oxidation ability owing to the highly negative CB edge and highly positive VB edge. $LaFeO_3$-based uncommon heterojunction is very useful and can be utilized in various reduction reactions. In $LaFeO_3$-based uncommon heterojunction, the semiconductor 1 could be excited under visible-light to produce charge carriers, while the semiconductor 2 (wide bandgap semiconductor i.e. TiO_2, ZnO, SnO_2, etc) can't be excited upon exposure to visible light as depicted in **Fig. 8(d)**. In such kind of heterojunctions, the visible light excited HLEEs of $LaFeO_3$ would move to the CB of wide band gap semiconductors for reduction reactions. In the meantime, the VB holes of $LaFeO_3$ would participate in oxidation reactions. This will drastically improve the charge carriers separation efficiency, leading to the enhanced activities of $LaFeO_3$.

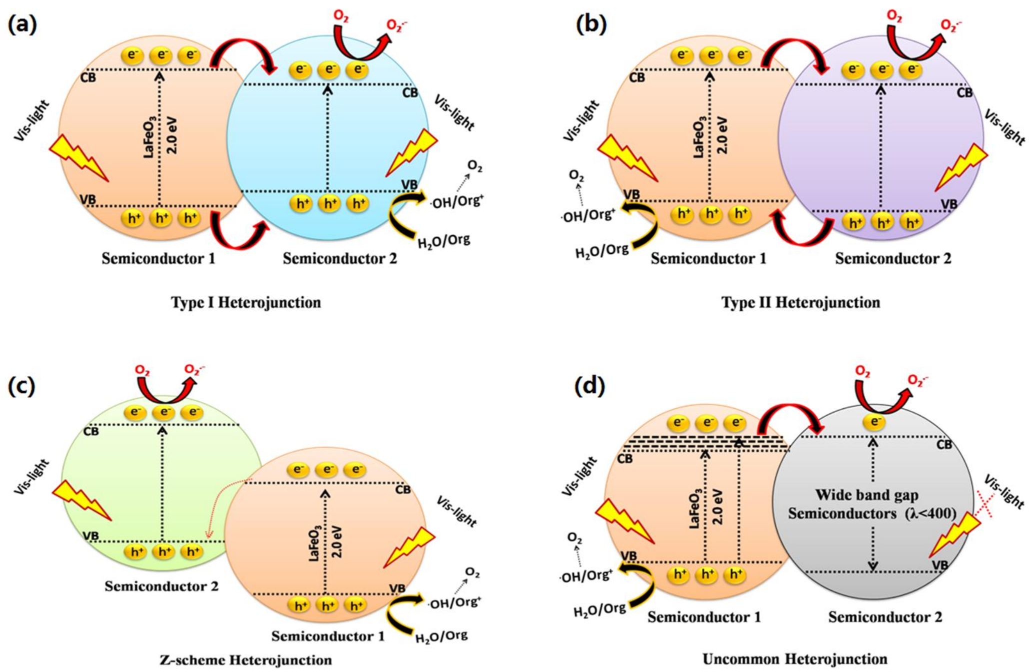

Fig. 8 Schematic of the four different kinds of heterostructures band alignments: Type I (a), Type II (b), Z-scheme (c), and uncommon (d).

Summary of several most recent publications on $LaFeO_3$-based heterostructures and their photocatalytic activity evaluation are shown in Table 2.

Table 2 Typical examples of $LaFeO_3$-based type I, type II, Z-scheme, and uncommon heterojunctions.

$LaFeO_3$-based composites	**Types**	**Photocatalytic reactions**	**Reference (Year)**
$Ag_2CrO_4/LaFeO_3$	Type II	RhB degradation	[237](2020)
$Ag/LaFeO_3$		RhB degradation	[238](2017)

$Au/LaFeO_3/Cu_2O$	Z-scheme	RhB degradation	[239](2020)
$CdS/LaFeO_3$	Type II	MB, RhB, MO degradation	[240](2019)
CdS QDs/$LaFeO_3$	Type II	H_2 evolution & RhB degradation	[241](2020)
CeO_2-$LaFeO_3$	Core-shell	NNK degradation	[242](2016)
$CuO/LaFeO_3$	Type I	RhB degradation	[243](2018)
Er^{+3}-$LaFeO_3/MgO$		CO_2 conversion	[244](2020)
Fe^{3+}-$La_2CuO_4/LaFeO_3$		Glycerol conversion	[245](2019)
α-$Fe_2O_3/LaFeO_3$	Type-II	MB degradation	[246](2020)
$LaFeO_3/Ag_2CO_3$	Z-scheme	RhB & p-Chlorophenol degradation	[247](2019)
$LaFeO_3$/Diatomite		Ciprofloxacin degradation	[244](2020)
$LaFeO_3$/CdS/C QDs	Type-II	H_2 evolution	[248](2020)
$LaFeO_3$/g-C_3N_4	Z-scheme	MO degradation	[249](2018)
$LaFeO_3$/g-C_3N_4	Z-scheme	H_2 evolution	[250](2017)
$LaFeO_3$/g-C_3N_4	Z-scheme	Oxytetracycline	[251](2020)
$LaFeO_3$-RGO-NiO		H_2 evolution, Congo-red degradation	[252](2021)
$LaFeO_3$/montmorillonite		RhB degradation	[93](2015)
$LaFeO_3$/rGO		H_2 evolution	[253](2017)
$LaFeO_3$–rGO		MB & RhB degradation	[254](2016)
$LaFeO_3$–rGO		MB degradation	[255](2018)
$LaFeO_3$/AgBr	Z-scheme	RhB degradation	[256](2018)
$LaFeO_3/Bi_3NbO_7$	Type II	Cr(Ⅵ) reduction	[257](2020)
$LaFeO_3$/g-C_3N_4	Z-scheme	H_2 evolution & MB degradation	[258](2017)
$LaFeO_3$/g-C_3N_4	Z-scheme	RhB and 4-CP degradation	[259](2019)
$LaFeO_3$-$SrTiO_3$	Uncommon	NO conversion	[260](2017)
$LaFeO_3/ZnIn_2S_4$	Type II	MO degradation	[261](2019)

$LaFeO_3@TiO_2$	Core-shell	Myclobutanil pesticide degradation	[262](2020)
$LaFeO_3$-TiO_2	Type II	MB degradation	[263](2019)
$LaFeO_3$-TiO_2	Type II	MO degradation	[264](2017)
$MoS_2/LaFeO_3$	Type I	H_2 evolution & RhB degradation	[265](2020)
$NiS/LaFeO_3/g\text{-}C_3N_4$	Z-scheme	H_2 evolution	[266](2017)
$NiS/LaFeO_3$	Z-scheme	MO degradation	[267](2020)
Ru-$LaFeO_3/Fe_2O_3$		Glucose degradation, H_2 evolution	[268](2018)
$LaFeO_3$/BiOBr	Z-scheme	RhB degradation	[269](2020)
$LaFeO_3/g\text{-}C_3N_4$	Z-scheme	Brilliant Blue degradation	[270](2018)
$g\text{-}C_3N_4/Ag/LaFeO_3$	Z-scheme	RhB degradation	[271](2019)
TiO_2/RGO/$LaFeO_3$	Z-scheme	H_2 evolution	[272](2019)
SnO_2/yolk-shell $LaFeO_3$	Uncommon	2,4-DCP degradation	[273](2020)
$TiO_2/LaFeO_3$		MB degradation	[274](2012)
Zn/Cr-$LaFeO_3$	Type II	H_2 evolution	[275](2017)
$g\text{-}C_3N_4/LaFeO_3$	Z-scheme	RhB degradation	[276](2018)
$LaFeO_3/SnS_2$	Z-scheme	Tetracycline degradation	[277](2019)
$TiO_2/LaFeO_3$	Uncommon	Acetaldehyde & Phenol degradation	[278](2016)
$TiO_2/LaFeO_3$	Uncommon	RhB degradation	[279](2011)
TiO_2/N-doped $LaFeO_3$	Uncommon	CO_2 conversion & 2,4-DCP degradation	[104](2016)
ZnO/Bi-doped $LaFeO_3$	Uncommon	CO_2 conversion & 2,4-DCP degradation	[105](2018)
$SrO/LaFeO_3$	Uncommon	CO_2 conversion & 2,4-DCP degradation	[280](2019)

6.2.1 $LaFeO_3$-based Type-I Heterojunctions

In $LaFeO_3$-based type-I heterojunction, the CB of $LaFeO_3$ should be more negative and its VB should be more positive than the CB and VB potentials of the coupled semiconductor. Thus, the photoinduced electrons and holes of $LaFeO_3$ would respectively migrate to CB and VB of the coupled semiconductor. As a result, the reduction and oxidation reactions of the type-I composites will occur on the surface of a coupled semiconductor having low redox potentials. This significantly suppresses the redox ability of the fabricated type-I heterojunctions. For example, Soltanabadi *et al.*[243] reported CuO/$LaFeO_3$ composites synthesized via a sol-gel route. The characteristic XRD peaks of CuO can be clearly observed in the CuO/$LaFeO_3$ composites (see **Fig. 9(a)**). The photocatalytic activity of the catalysts was appraised for RhB dye degradation under visible light irradiation. The photocatalytic activity of $LaFeO_3$ drastically enhanced with increase in the amount of CuO content and the highest activity was observed for 50%CuO/$LaFeO_3$ composite (see **Fig. 9(b)**). This was accredited to the remarkably enhanced charge separation in the CuO/$LaFeO_3$ composite. The charge carrier's separation was motivated by the internal re-assembly that rebuilds the electric field in the composite. Consequently, the charge carrier's recombination has decreased which leads to the electrons accumulation in CB of CuO and holes accumulation in the VB of $LaFeO_3$ (see **Fig. 9(c)**). Recently, Acharya *et al.*[265] synthesized mesoporous $LaFeO_3$ through nanocasting method and then coupled it with molybdenum disulfide (MoS_2). The TEM image of the composite (**Fig. 9(d)**) revealed the presence of sheets of MoS_2 and the porous $LaFeO_3$ particles. The HRTEM micrograph (**Fig. 9(e)**) revealed distinct lattice fringes related to the MoS_2 (0.62 nm) and $LaFeO_3$ (0.28 nm). The photocatalytic activity of the composites was appraised by H_2O reduction to evolve H_2 under visible light. The H_2 evolution activity of $LaFeO_3$ was remarkably improved after coupling MoS_2, and the optimized 1wt%MoS_2/$LaFeO_3$ composite produced 1132 mmol $h^{-1}g^{-1}$ of H_2 which is much greater than that produced by bare $LaFeO_3$. This enhanced activity was due to the mesoporous nature and the improved charge separation in the composite. As suggested, the S-dangling bonds at the MoS_2 surface were responsible for capturing the H_2O molecules, which produced H^+ and OH^- upon dissociation, and the H^+ ions then reduced to H_2 by the interaction with CB electrons of MoS_2 (**see Fig. 9(f)**). Thus, the charge separation and transfer mechanism extended the lifetime of photo-induced charges of the MoS_2/$LaFeO_3$ composite which resulted in the improved photocatalytic performance.

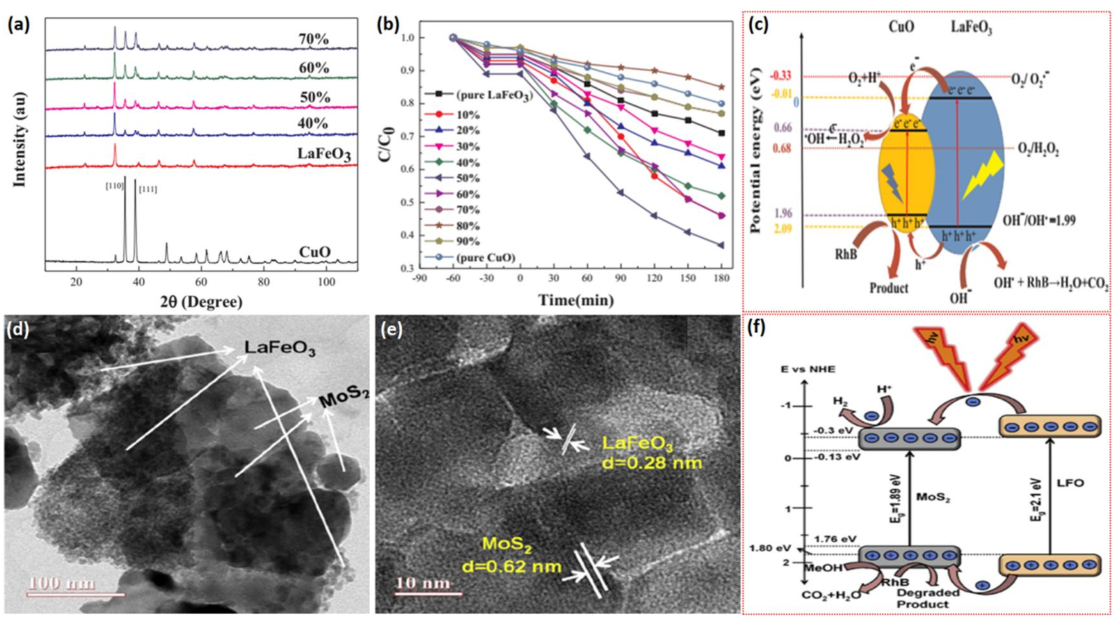

Fig. 9 XRD patterns (a), and visible light catalytic activity for RhB degradation (b) of the $LaFeO_3$, CuO and CuO/$LaFeO_3$ composites. Schematic for band structure, charge transfer, and the photocatalytic

processes over $CuO/LaFeO_3$ composites (c). Adapted with permission from ref. [243] Copyright 2018, Elsevier. TEM micrograph (d), HRTEM micrograph (e), and photocatalytic charge transfer mechanism of $MoS_2/LaFeO_3$ composite (f). Adapted with permission from ref. [265] Copyright 2020, Elsevier.

6.2.2 $LaFeO_3$-based Type-II Heterojunctions

The performance of $LaFeO_3$ photocatalyst is severely influenced by the poor holes collection from body to the surface, although it has a suitable visible light absorption. Specifically, the short diffusion-length of the holes in bulk $LaFeO_3$ strictly limits its performance, because 'B' site cation (Fe^{3+}) decides the redox processes and electronic behavior. Actually, to hinder the charge recombination in $LaFeO_3$, this problem can be solved by fabricating heterojunctions with proper band gap semiconductors. A proper band structure is a key deliberation to choose the second photocatalyst for constructing $LaFeO_3$-based type-II heterojunctions. Ye *et al.*[237] reported the fabrication of $Ag_2CrO_4/LaFeO_3$ composite via a chemical precipitation technique. The XRD patterns of the $Ag_2CrO_4/LaFeO_3$ composites (**Fig. 10(a)**) revealed additional peak at 2θ of 31°, corresponding to the Ag_2CrO_4 particles. The color of $LaFeO_3$, $Ag_2CrO_4/LaFeO_3$ and Ag_2CrO_4 samples can be observed in **Fig. 10(a)** inset. The decoration of Ag_2CrO_4 nanoparticles onto the $LaFeO_3$ surface could be observed from TEM micrograph (**Fig. 10(b)**). The diffraction spots in the selected area electron diffraction (SAED) patterns (**Fig. 10(b)** inset) clarified the perfect crystallinity of the composite. The lattice fringes of $LaFeO_3$ (d = 0.397 nm) and that of the Ag_2CrO_4 (d = 0.287 nm) could be observed from the HRTEM image (**Fig. 10(c)**). The photo-Fenton degradation activity of the composites was investigated for RhB dye under simulated light in the presence of H_2O_2. The

10%Ag_2CrO_4/$LaFeO_3$ composites exhibited high photo-Fenton activity, which was approximately 3.1 and 2.5-time greater in comparison to that of pure $LaFeO_3$ and Ag_2CrO_4, respectively (see **Fig. 10(d)**). As investigated, under light irradiations, the photo-induced electrons of $LaFeO_3$ will transport to the CB of Ag_2CrO_4 due to the highly negative CB potential of $LaFeO_3$, and on the contrary, photo-induced holes in VB of Ag_2CrO_4 will transfer to the VB of $LaFeO_3$ due to the highly positive VB level of Ag_2CrO_4 (see **Fig. 10(e)**). The charger carrier transfer and separation lead to the superior photoactivities of the composites. In another work, Acharya *et al.*[241] reported the fabrication of CdS QDs/$LaFeO_3$ composites via deposition method. The TEM micrograph of the composite (**Fig. 10(f)**) revealed uniform distribution of CdS QDs onto the surface of $LaFeO_3$. The HRTEM micrograph (**Fig. 10(g)**) clearly revealed two distinct lattice fringes related to the CdS QDs and $LaFeO_3$ nanoparticles. The composites photo-activity was appraised by H_2 generation upon exposure to visible light radiation with the aid of a sacrificial agent (CH_3OH). The H_2 evolved over the CdS QDs/$LaFeO_3$ composites was remarkably enhanced. The amount optimized 1wt%CdS QDs/$LaFeO_3$ composite produced 935.5 μmol h^{-1} of H_2, which was much obvious compared to that of the bare $LaFeO_3$ catalyst (i.e. 237.5 μmol h^{-1}). Upon exposure to visible light radiations, charge carriers were produced in both components of the CdS QDs/$LaFeO_3$ composite photocatalyst. According to the highly negative CB potential of CdS QDs, the photo-induced electrons were transferred to the CB of $LaFeO_3$, employing an interface where they contributed to the H_2 generation (see **Fig. 10(h)**). It should be noted that coupling of CdS QDs shrank the charge carrier's recombination in $LaFeO_3$. Consequently, the H_2

generation activity was remarkably improved. Thus, it is concluded that constructing type-II heterojunctions are favorable for enhancement in charge carriers and the photo-activities. Remarkably, the efficient utilization of solar energy, abundant surface active sites, and the interfacial junction in type-II system are crucial for the improvement in photo-activities.

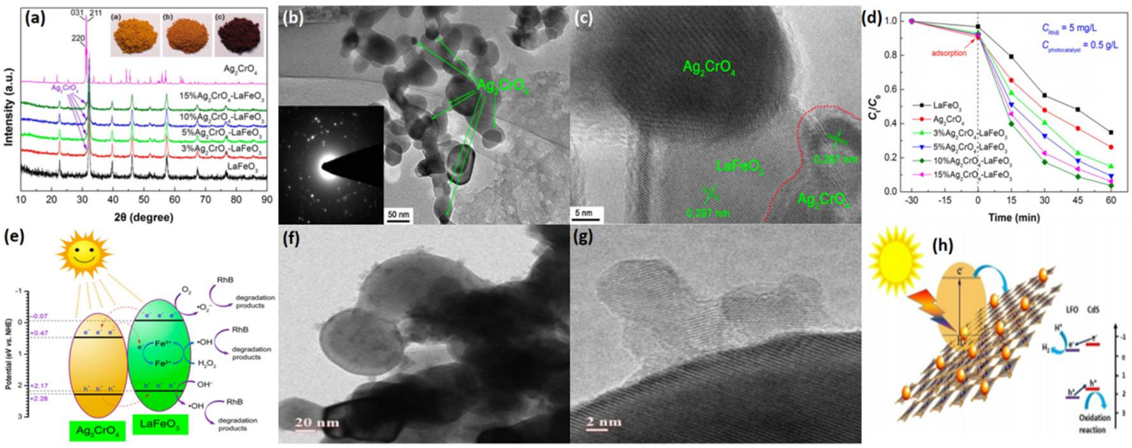

Fig. 10 XRD patterns with color of the $LaFeO_3$, $Ag_2CrO_4/LaFeO_3$ and Ag_2CrO_4 samples as inset (a), TEM image (b) and HRTEM image (c) of the $Ag_2CrO_4/LaFeO_3$ composite. Visible light catalytic activity of the samples for RhB dye degradation (d), and schematic for charge transport and separation and the photocatalytic reactions over the $Ag_2CrO_4/LaFeO_3$ composite (e). Reproduced with permission from ref. [237] Copyright 2020, Taylor & Francis. TEM image (f), HRTEM image (g), and the schematic for charge transfer and separation and the photocatalytic processes over the CdS QDs/$LaFeO_3$ composite (h). Adapted with permission from ref. [241] Copyright 2020, Wiley-VCH.

6.2.3 $LaFeO_3$-based Z-scheme Heterojunctions

It is highly preferred to investigate the suitable photocatalytic systems with adequate light absorption and proficient charge carrier's separation. Luckily, Z-scheme systems could solve majority of the problems related to the efficient photocatalysis to a certain degree, because Z-scheme systems not only acquire outstanding charge separation ability, but also maintain high redox ability of the electron-hole pairs. In Z-scheme systems, the photo-generated electrons of semiconductor 1 (with weak reduction power) facilitate direct recombination with the photo-generated holes of semiconductor 2 (with weak oxidizing power). Meanwhile, the photo-generated electrons of semiconductor 2 posses strong reduction ability, while the photo-generated holes of semiconductor 1 possess strong oxidation ability for efficient photocatalytic reactions[277]. Yet, the design of an appropriate low cost, environmental friendly and highly stable Z-scheme system for efficient visible light photocatalysis has attracted worldwide scientific attention. For instance, Xu et al. fabricated core-shell $LaFeO_3$/g-C_3N_4 Z-scheme heterojunction via a facile method as depicted in **Fig. 11(a)**. The TEM image (**Fig. 11(b)**) reveals the presence of g-C_3N_4 shell. The lattice fringes of $LaFeO_3$ and the g-C_3N_4 shell can be clearly observed from the HRTEM image (**Fig. 11(c)**). The charge transfer reveals a Z-scheme as shown in **Fig. 11(d)**. Thus, the Z-scheme system has been proven to be an important strategy to improve the redox activity of heterostructures. Ye *et al.*[276] reported the process of fabricating g-C_3N_4/$LaFeO_3$ Z-type heterojunction by simply calcination of mixed g-C_3N_4 and $LaFeO_3$ particles. The TEM image (**Fig. 11(e)**) clearly demonstrates particles of $LaFeO_3$ onto the CN surface, while the lattice fringes of $LaFeO_3$ can be observed through HRTEM image (**Fig. 11(f)**). The photo-Fenton activity of the catalysts was appraised for RhB degradation under simulated light as shown in **Fig. 11(g)**. The 15%g-C_3N_4/$LaFeO_3$ composites exhibited high performance for photo-Fenton RhB degradation. The increase in activity was accredited to the significant charge carrier's separation due to Z-scheme electron-transfer mechanism (see **Fig. 11(h)**) in g-$C_3N_4/LaFeO_3$ composite. Under simulated light irradiations, charge carriers were generated in both components $LaFeO_3$ and g-C_3N_4 of the composite. The photogenerated electrons of $LaFeO_3$ were recombined with the photo-induced holes in the VB of g-C_3N_4. Meanwhile, the induced VB holes of $LaFeO_3$ and CB electrons of g-C_3N_4 participated in the photocatalytic processes. Thus, the g-$C_3N_4/LaFeO_3$ nanocomposites exhibited superior photocatalytic activity compared to the single $LaFeO_3$ and g-C_3N_4 components. Among the $LaFeO_3$-based Z-scheme heterojunctions, the dual Z-scheme exhibit higher activity than the normal Z-scheme systems. Zhang *et al.*[281] reported dual Z-scheme AgI/$LaFeO_3$/g-C_3N_4 composite that was fabricated via an ultrasonic assisted hydrothermal technique. The XRD patterns (**Fig. 11(i)**) revealed the peaks related to $LaFeO_3$, AgI and g-C_3N_4 in the composite, and their distinct particles can be observed from TEM image (**Fig. 11(j)**). The visible light photo-activity of the dual Z-scheme composite was appraised for norfloxacin degradation as shown in **Fig. 11(k)**. About 95% of the norfloxacin degradation was accomplished in 2h by the AgI/$LaFeO_3$/g-C_3N_4 nanocomposite which was accredited to the synergistic-effect produced as a result of the activation of a well-aligned three components system. According to the suggested mechanism (see **Fig. 11(l)**), upon exposure to visible light radiations, the excited electrons in the CB of $LaFeO_3$ would recombine with the excited VB holes of g-C_3N_4 and AgI catalysts. The migration of photo-induced carriers causes the electrons to stay in the CB of g-C_3N_4 and AgI, and holes accumulate in the VB of $LaFeO_3$. The electrons excited to the CB of g-C_3N_4 and AgI could reduce O_2 to $O_2^{\bullet-}$ due to their more negative CB levels than -0.33 V. Thus, this dual Z-type migration-pattern would be of great significance for improving the efficiency of $LaFeO_3$ for photodegradation of various pollutants.

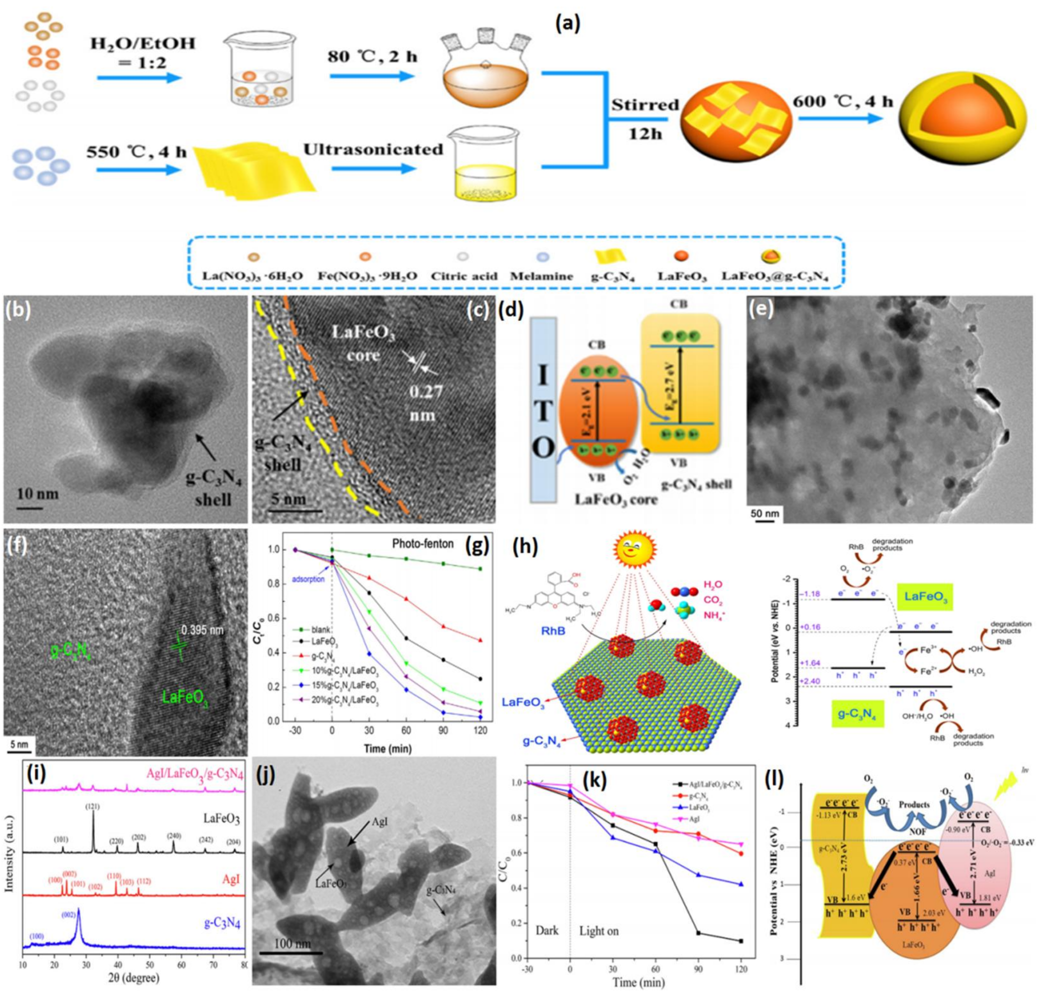

Fig. 11 (a) Scheme for the synthesis, TEM micrograph (b), HRTEM micrograph (c) and charge carriers transfer mechanism (d) of the $LaFeO_3$/g-C_3N_4 Z-scheme core-shell heterojunction. Adapted with permission from ref.[282] Copyright 2020, Elsevier. TEM image (e) and HRTEM image (f) of g-C_3N_4/$LaFeO_3$ Z-scheme composite. (g) The photo-Fenton activities of g-C_3N_4, $LaFeO_3$ and the g-

$C_3N_4/LaFeO_3$ composites. Schematic for charge separation and photocatalytic processes over g-$C_3N_4/LaFeO_3$ Z-scheme composite (h). Reproduced with permission from ref.[276] Copyright 2018, Elsevier. XRD patterns (i), TEM image (j), norfloxacin degradation activities (k) and the schematic for charge transfer mechanism and photocatalytic processes over the dual Z-scheme $AgI/LaFeO_3/g\text{-}C_3N_4$ hetero-junction (l). Adapted with permission from ref.[281] Copyright 2020, Elsevier.

6.2.4 $LaFeO_3$-based Uncommon Heterojunctions

Fortunately, uncommon heterojunctions are more beneficial than the type-I, type-II, and Z-scheme heterojunctions because of the strong reduction and oxidation ability due to the drastically promoted charge separation. In our previous report,[278] we fabricated TiO_2/porous $LaFeO_3$ nanocomposites via a wet chemical route. The activities of the composites were appraised by acetaldehyde and phenol degradations under visible light irradiations (see **Fig. 12(a)**). It should be noted that the introduction of TiO_2 greatly improved the activities of $LaFeO_3$ for gas-phase acetaldehyde and liquid-phase phenol degradations and the highest activities were observed for the optimized 9wt%$TiO_2/LaFeO_3$ composite. The optimized sample produced highest amount of hydroxyl radical as shown in **Fig. 12(b)**. Thus, it was confirmed that the enhanced photoactivity was due to the improved charge separation and transfer as described in **Fig. 12(c)**. Recently our group [273] reported the synthesis of SnO_2/yolk-shell $LaFeO_3$ nanocomposites via a wet chemical method. In the SnO_2/yolk-shell $LaFeO_3$ nanocomposites, the SnO_2 nanoparticles were used as photoelectron modulators. The yolk-shell structure could be observed from the TEM image (see **Fig. 12(d)**). The distinct lattice fringes of SnO_2 and $LaFeO_3$ could be observed from HRTEM image (see **Fig.**

12(e)). The surface photovoltage spectra (**Fig. 12(f)**) revealed that charge separation in the optimized sample was much significant. The composites activity was evaluated for degradation of 2,4-dichlorophenol. The optimized 10%SnO_2/yolk-shell $LaFeO_3$ composites showed 1.6-time enhanced activity for degradation of 2,4-dichlorophenol pollutants in comparison to the yolk-shell $LaFeO_3$ upon exposure to visible light radiations (see **Fig. 12(g)**). According to the proposed mechanism (see **Fig. 12(h)**), the SnO_2 acted as a photoelectron modulator for improvement of charge carriers separation and the h^+ was a pioneer specie for 2,4-dichlorophenol degradation. This exceptional charge carrier separation lead to the remarkably improved photo-activities for degradation of 2,4-DCP. Beside SnO_2, we also utilized SrO as a suitable energy platform for accepting HLEEs of $LaFeO_3$ and fabricated SrO/$LaFeO_3$ composites via a one-pot carbon sphere template route[280]. The TEM image (**Fig. 12(i)**) revealed porous morphology of the composite. The HRTEM image (**Fig. 12(j)**) represented two distinct lattice fringes corresponding to the SrO and $LaFeO_3$. The composites photo-activities were appraised for CO_2 conversion as shown in **Fig. 12(k)**. The CO_2 conversion over the optimized composite was much obvious compared to the porous $LaFeO_3$. It was confirmed that the improved photoactivities were accredited to the charge separation enhancement as a result of the visible light excited HLEEs transfer to the CB of SrO (see **Fig. 12(l)**). Thus, the newly designed uncommon heterojunction systems are more beneficial for various redox reactions. Though the activities of $LaFeO_3$ were improved, however, the results were still not satisfactory for practical applications.

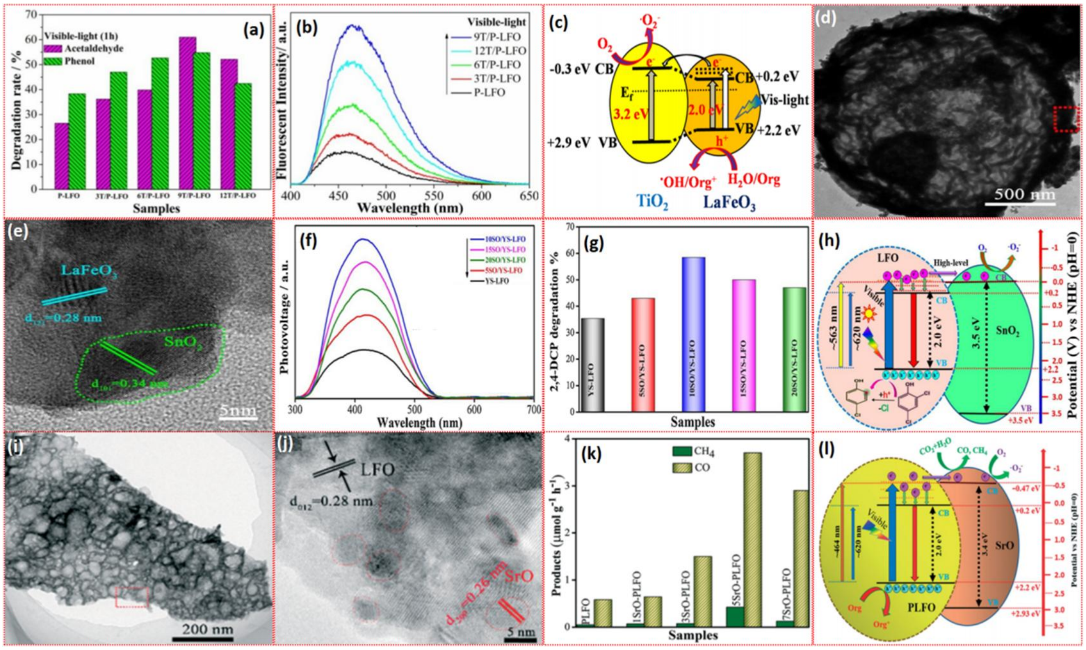

Fig. 12 Visible light catalytic activities for phenol and acetaldehyde degradation (a), and the fluorescence spectra (b) of $LaFeO_3$ and TiO_2/porous $LaFeO_3$ composites. Schematic for charge carriers transfer mechanism and the photocatalytic phenomenon in TiO_2/porous $LaFeO_3$ nanocomposite (c). Reproduced with permission from ref. [278] Copyright 2016, MDPI. TEM micrograph (d), and HRTEM micrograph (e) of yolk-shell SnO_2/$LaFeO_3$ composites. Surface photovoltage spectra (f) and 2,4-dichlorophenol activity (g) of porous $LaFeO_3$ and the yolk-shell SnO_2/$LaFeO_3$ composites. Schematic for charge transfer mechanism and photocatalytic processes over the SnO_2/yolk-shell $LaFeO_3$ composite (h). Adapted with permission from ref. [273] Copyright 2020, Elsevier. TEM image (i) and HRTEM image (j) of SrO/porous $LaFeO_3$ composite. CO_2 reduction activity of porous $LaFeO_3$ and SrO/porous $LaFeO_3$ composites (k). Schematic for charge transfer mechanism and photocatalytic processes over the SrO/porous $LaFeO_3$ composite (l). Adapted with permission from ref. [280] Copyright 2019, The Royal Society of Chemistry.

In order to achieve superior results, firstly we introduced pores in $LaFeO_3$ via carbon nanospheres-template assisted route and then doped nitrogen into its crystal lattice [104]. Finally, we coupled TiO_2 with the N-doped porous $LaFeO_3$ using the wet-chemical technique. The surface photovoltage spectra (**Fig. 13(a)**) revealed that charge separation in composites is remarkably improved especially for the optimized 6wt%TiO_2/N-doped porous $LaFeO_3$ composite. The photoactivities of the catalysts were appraised by the CO_2 conversion and degradation of 2,4-dichlorophenol under visible light. The 2,4-DCP degradation activity of the optimized 6wt%TiO_2/N-doped porous $LaFeO_3$ composite was significantly enhanced compared to that of the porous $LaFeO_3$ (see **Fig. 13(b)**). It was investigated that the HLEEs in the CB of TiO_2 induced reduction processes with carbon dioxide and oxygen and produced CH_4 and CO, and/or $O_2^{\bullet-}$, respectively (see **Fig. 13(c)**). On the other hand, the holes in VB of N-doped $LaFeO_3$ initiated oxidation processes with H_2O and produced •OH or O_2. To confirm the role of wide band gap photocatalysts in uncommon heterojunctions, we replaced TiO_2 with ZnO. This is because the photogenerated electron of $LaFeO_3$ possesses low energy to initiate reduction processes thermodynamically. However, when a wide band gap semiconductor with a suitable energy level platform is coupled with $LaFeO_3$ and the composite is exposed to visible light radiations, the generated HLEEs of $LaFeO_3$ would transfer thermodynamically to the CB of semiconductor with wide band gap leading to superior charge separation and visible light performance. To effectively employ the excited HLEEs of $LaFeO_3$ in photocatalysis, we fabricated ZnO coupled Bi-doped $LaFeO_3$ composites [105]. The TEM image of the ZnO/Bi-$LaFeO_3$ composite (see **Fig. 13(d)**) revealed porous morphology. The HRTEM image revealed two distinct lattice fringes related to the ZnO and $LaFeO_3$ (see **Fig. 13(e)**). The surface photovoltage spectra (**Fig. 13(f)**) and the transient photovoltage spectra (**Fig. 13(g)**) revealed that 5%ZnO/Bi-$LaFeO_3$ sample exhibited prolong lifetime of charge separation. The photoactivities of the composites were appraised by 2,4-dichlorophenol degradation and CO_2 reduction. The photocatalytic activity of the optimized 5%ZnO/Bi-$LaFeO_3$ composite for 2,4-dichlorophenol was enhanced by 2.75-time compared to that of the porous $LaFeO_3$ (see **Fig. 13(h)**). Similarly, the activity of optimized composite for CO_2 reduction was significantly improved in comparison to that of the porous $LaFeO_3$ (see **Fig. 13(i)**). The superior visible light catalytic activities of the nanocomposites were accredited to the enlarged surface area due to porous structure, to the extended visible light response by Bi incorporated new energy levels, and to the significant use of visible-light-induced electrons by ZnO coupling. As expected, the transferred HLEEs to the CB of ZnO would have enough energy to initiate reduction processes with O_2 and CO_2 respectively to generate $O_2^{\bullet-}$ and/or CH_4 and CO (see **Fig. 13(j)**). Besides, the VB holes can induce oxidation processes with H_2O to generate $^{\bullet}OH$. Therefore, it is highly significant to use the photo-induced HLEEs of perovskite-type $LaFeO_3$ to make its visible light catalytic performance more realistic for environment protection and solar fuel generation.

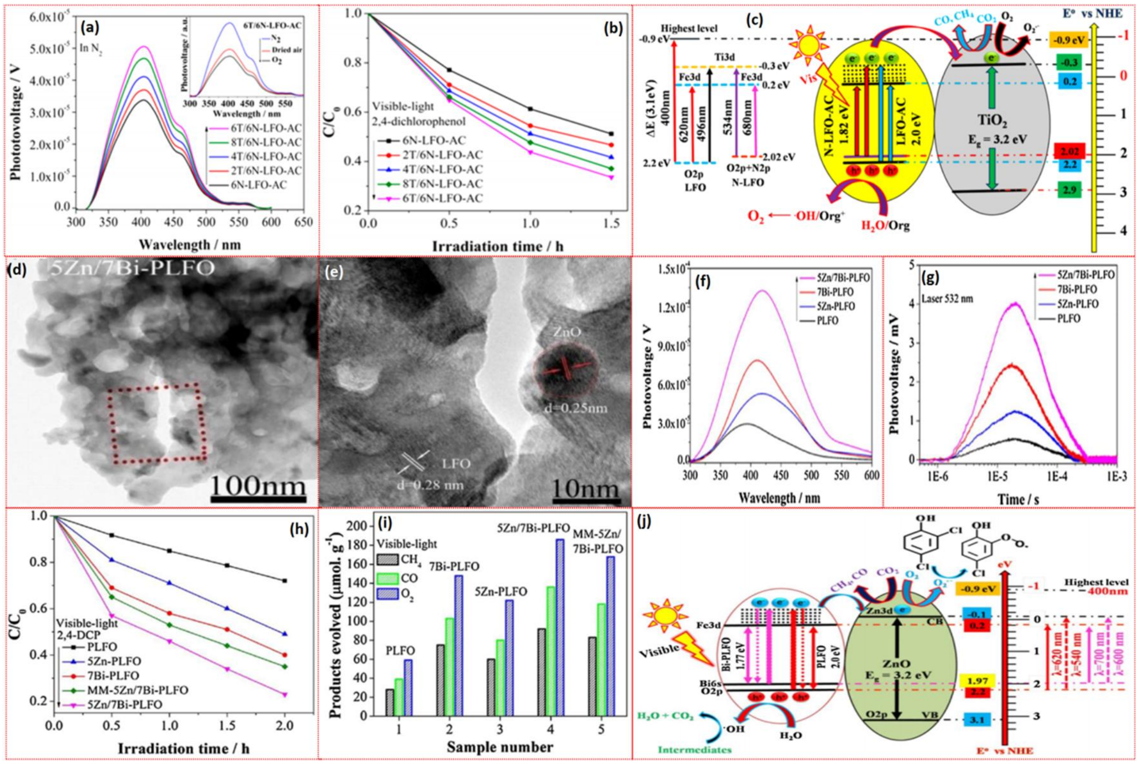

Fig. 13 Surface photovoltage spectra (a), and the 2,4-DCP degradation activities (b) of the TiO_2/N-doped porous $LaFeO_3$ composites. Schematic for the energy band structure, charge carriers transfer mechanism, and photocatalytic processes in the TiO_2/N-doped porous $LaFeO_3$ composite (c). Adapted with permission from ref. [104] Copyright 2016, The American Chemical Society. TEM image (d) and HRTEM image (e) of the 5Zn/Bi-$LaFeO_3$ composite. Surface photovoltage spectra (f), transient photovoltage spectra (g), 2,4-DCP activity (h) and CO_2 conversion activity (i) of the samples. Schematic for the energy band structure and charge transfer mechanism in the 5Zn/Bi-$LaFeO_3$ nanocomposite (j). Adapted with permission from ref. [105] Copyright 2018, Elsevier.

7. Conclusion and Perspectives

In this review, we have comprehensively summarized the research progress in the design, development, and application of perovskite-type $LaFeO_3$ materials in the field of photocatalysis. First, we covered the history and basic principles of photocatalysis in terms of oxidation and reduction reactions, which was followed by the history, applications, shortcomings, and modification strategies such as the nanostructure synthesis, doping, and heterostructures formation, to enhance the photocatalytic activity of $LaFeO_3$. The idea of uncommon heterojunctions was also discussed where the $LaFeO_3$ produces charge carriers, upon exposure to visible light radiations. This idea of uncommon heterojunction is beyond the conventional type-I, type-II, and Z-scheme heterojunctions and much crucial for efficient photocatalysis. We proposed that the design of nanostructure can remarkably improve the surface area of $LaFeO_3$ that can efficiently perform photocatalysis. In summary, the modification strategies such as nanostructuring, elemental doping, and heterojunctions formation can significantly improve the photocatalytic performance of $LaFeO_3$, by increasing specific surface area, extending light absorption, suppressing charge carriers recombination, and efficient utilization of electrons.

The important points for future consideration are given below:

1. As for the small surface area and large particles size problems, the reaction time and reaction temperature should be controlled. Further, different templates such as carbon nanospheres and polystyrene spheres can be used and the control sized porous materials can be easily prepared.

2. In order to promote the adsorption of O_2 onto the surface of photocatalysts, modification with inorganic acids is highly recommended.

3. Doping of metal and non-metal elements can be functional to promote light absorption and suppressing charge carriers recombination via the generated new energy states.

4. As for pollutant degradation reactions, the key step to promote the photocatalytic efficiency of photocatalysts is to enhance its charge carrier's separation. One common strategy that is widely employed is to fabricate type-II, Z-scheme and uncommon heterojunctions. This can remarkably improve the photocatalytic activities of the photocatalysts.

Acknowledgements

The work was financially supported by the Ministry of Science and Technology of China (Grant No. 2018YFA0702100), the National Natural Science Foundation of China (Grant No. 11874169, 51972129), and the National Key R&D Program of China (Grant No. 2017YFE0120500), the Key Research and Development Program of Hubei (Grant No. 2020BAB079), and the South Xinjiang Innovation and Development Program of Key Industries of Xinjiang Production and Construction Corps (Grants No. 2020DB002). C.D.W. acknowledges the Hubei "Chu-Tian Young Scholar" program.

References

[1] M. Höök, X. Tang, Depletion of fossil fuels and anthropogenic climate change—A review, Energy Policy, 52 (2013) 797-809.

[2] S. Bilgen, Structure and environmental impact of global energy consumption, Renewable and Sustainable Energy Reviews, 38 (2014) 890-902.

[3] M. Humayun, W. Pi, Y. Yuan, L. Shu, J. Cao, A. Khan, Z. Zheng, Q. Fu, Y. Tian, W. Luo, A rational design of g-C3N4-based ternary composite for highly efficient H2 generation and 2,4-DCP degradation, Journal of Colloid and Interface Science, 599 (2021) 484-496.

[4] N. Armaroli, V. Balzani, The Future of Energy Supply: Challenges and Opportunities, Angewandte Chemie International Edition, 46 (2007) 52-66.
[5] S.C. Roy, O.K. Varghese, M. Paulose, C.A. Grimes, Toward Solar Fuels: Photocatalytic Conversion of Carbon Dioxide to Hydrocarbons, ACS Nano, 4 (2010) 1259-1278.
[6] M.D. Garba, M. Usman, S. Khan, F. Shehzad, A. Galadima, M.F. Ehsan, A.S. Ghanem, M. Humayun, CO2 towards fuels: A review of catalytic conversion of carbon dioxide to hydrocarbons, Journal of Environmental Chemical Engineering, 9 (2021) 104756.
[7] J. Schneider, M. Matsuoka, M. Takeuchi, J. Zhang, Y. Horiuchi, M. Anpo, D.W. Bahnemann, Understanding TiO2 Photocatalysis: Mechanisms and Materials, Chemical Reviews, 114 (2014) 9919-9986.
[8] P. Poizot, F. Dolhem, Clean energy new deal for a sustainable world: from non-CO2 generating energy sources to greener electrochemical storage devices, Energy & Environmental Science, 4 (2011) 2003-2019.
[9] I.U. Din, M. Usman, S. Khan, A. Helal, M.A. Alotaibi, A.I. Alharthi, G. Centi, Prospects for a green methanol thermo-catalytic process from CO2 by using MOFs based materials: A mini-review, Journal of CO2 Utilization, 43 (2021) 101361.
[10] R. Marschall, Semiconductor Composites: Strategies for Enhancing Charge Carrier Separation to Improve Photocatalytic Activity, Advanced Functional Materials, 24 (2014) 2421-2440.
[11] W. Tu, Y. Zhou, Z. Zou, Photocatalytic Conversion of CO2 into Renewable Hydrocarbon Fuels: State-of-the-Art Accomplishment, Challenges, and Prospects, Advanced Materials, 26 (2014) 4607-4626.
[12] M. Usman, A. Helal, M.M. Abdelnaby, A.M. Alloush, M. Zeama, Z.H. Yamani, Trends and Prospects in UiO-66 Metal-Organic Framework for CO2 Capture, Separation, and Conversion, The Chemical Record, n/a (2021).
[13] S. Cao, J. Low, J. Yu, M. Jaroniec, Polymeric Photocatalysts Based on Graphitic Carbon Nitride, Advanced Materials, 27 (2015) 2150-2176.

[14] I. Paramasivam, H. Jha, N. Liu, P. Schmuki, A Review of Photocatalysis using Self-organized TiO2 Nanotubes and Other Ordered Oxide Nanostructures, Small, 8 (2012) 3073-3103.

[15] F. Xu, Y. Shen, L. Sun, H. Zeng, Y. Lu, Enhanced photocatalytic activity of hierarchical ZnO nanoplate-nanowire architecture as environmentally safe and facilely recyclable photocatalyst, Nanoscale, 3 (2011) 5020-5025.

[16] X. Bai, L. Wang, R. Zong, Y. Lv, Y. Sun, Y. Zhu, Performance Enhancement of ZnO Photocatalyst via Synergic Effect of Surface Oxygen Defect and Graphene Hybridization, Langmuir, 29 (2013) 3097-3105.

[17] E.S. Jang, J.H. Won, S.J. Hwang, J.H. Choy, Fine Tuning of the Face Orientation of ZnO Crystals to Optimize Their Photocatalytic Activity, Advanced Materials, 18 (2006) 3309-3312.

[18] X. Wang, M. Liao, Y. Zhong, J.Y. Zheng, W. Tian, T. Zhai, C. Zhi, Y. Ma, J. Yao, Y. Bando, D. Golberg, ZnO Hollow Spheres with Double-Yolk Egg Structure for High-Performance Photocatalysts and Photodetectors, Advanced Materials, 24 (2012) 3421-3425.

[19] S. Wu, H. Cao, S. Yin, X. Liu, X. Zhang, Amino Acid-Assisted Hydrothermal Synthesis and Photocatalysis of SnO2 Nanocrystals, The Journal of Physical Chemistry C, 113 (2009) 17893-17898.

[20] S. Liu, G. Huang, J. Yu, T.W. Ng, H.Y. Yip, P.K. Wong, Porous Fluorinated SnO2 Hollow Nanospheres: Transformative Self-assembly and Photocatalytic Inactivation of Bacteria, ACS Applied Materials & Interfaces, 6 (2014) 2407-2414.

[21] S. Liu, K. Yin, W. Ren, B. Cheng, J. Yu, Tandem photocatalytic oxidation of Rhodamine B over surface fluorinated bismuth vanadate crystals, Journal of Materials Chemistry, 22 (2012) 17759-17767.

[22] S.-W. Cao, Z. Yin, J. Barber, F.Y.C. Boey, S.C.J. Loo, C. Xue, Preparation of Au-BiVO4 Heterogeneous Nanostructures as Highly Efficient Visible-Light Photocatalysts, ACS Applied Materials & Interfaces, 4 (2012) 418-423.

[23] J. Zhu, F. Fan, R. Chen, H. An, Z. Feng, C. Li, Direct Imaging of Highly Anisotropic Photogenerated Charge Separations on Different Facets of a Single BiVO4 Photocatalyst, Angewandte Chemie International Edition, 54 (2015) 9111-9114.
[24] H. Li, H. Yu, X. Quan, S. Chen, H. Zhao, Improved Photocatalytic Performance of Heterojunction by Controlling the Contact Facet: High Electron Transfer Capacity between TiO2 and the {110} Facet of BiVO4 Caused by Suitable Energy Band Alignment, Advanced Functional Materials, 25 (2015) 3074-3080.
[25] C.N. Van, W.S. Chang, J.-W. Chen, K.-A. Tsai, W.-Y. Tzeng, Y.-C. Lin, H.-H. Kuo, H.-J. Liu, K.-D. Chang, W.-C. Chou, C.-L. Wu, Y.-C. Chen, C.-W. Luo, Y.-J. Hsu, Y.-H. Chu, Heteroepitaxial approach to explore charge dynamics across Au/BiVO4 interface for photoactivity enhancement, Nano Energy, 15 (2015) 625-633.
[26] M. Xie, J. Bian, M. Humayun, Y. Qu, Y. Feng, L. Jing, The promotion effect of surface negative electrostatic field on the photogenerated charge separation of BiVO4 and its contribution to the enhanced PEC water oxidation, Chemical Communications, 51 (2015) 2821-2823.
[27] W.J. Jo, J.-W. Jang, K.-j. Kong, H.J. Kang, J.Y. Kim, H. Jun, K.P.S. Parmar, J.S. Lee, Phosphate Doping into Monoclinic BiVO4 for Enhanced Photoelectrochemical Water Oxidation Activity, Angewandte Chemie International Edition, 51 (2012) 3147-3151.
[28] H. Zhang, H. Li, Z. Wang, Z. Zheng, P. Wang, Y. Liu, X. Zhang, X. Qin, Y. Dai, B. Huang, Fabrication of BiVO4 photoanode consisted of mesoporous nanoparticles with improved bulk charge separation efficiency, Applied Catalysis B: Environmental, 238 (2018) 586-591.
[29] X. Zhang, Z. Ai, F. Jia, L. Zhang, X. Fan, Z. Zou, Selective synthesis and visible-light photocatalytic activities of BiVO4 with different crystalline phases, Materials Chemistry and Physics, 103 (2007) 162-167.
[30] Z. Li, Y. Qu, K. Hu, M. Humayun, S. Chen, L. Jing, Improved photoelectrocatalytic activities of BiOCl with high stability for water oxidation and MO degradation by coupling RGO and modifying phosphate groups to prolong carrier lifetime, Applied Catalysis B: Environmental, 203 (2017) 355-362.

[31] B. Kiss, T.D. Manning, D. Hesp, C. Didier, A. Taylor, D.M. Pickup, A.V. Chadwick, H.E. Allison, V.R. Dhanak, J.B. Claridge, J.R. Darwent, M.J. Rosseinsky, Nano-structured rhodium doped SrTiO3–Visible light activated photocatalyst for water decontamination, Applied Catalysis B: Environmental, 206 (2017) 547-555.
[32] L.F. da Silva, J.-C. M'Peko, J. Andrés, A. Beltrán, L. Gracia, M.I.B. Bernardi, A. Mesquita, E. Antonelli, M.L. Moreira, V.R. Mastelaro, Insight into the Effects of Fe Addition on the Local Structure and Electronic Properties of SrTiO3, The Journal of Physical Chemistry C, 118 (2014) 4930-4940.
[33] X. Wu, X. Wang, J. Li, G. Zhang, Boosting molecular oxygen activation of SrTiO3 by engineering exposed facets for highly efficient photocatalytic oxidation, Journal of Materials Chemistry A, 5 (2017) 23822-23830.
[34] S. Taibl, G. Fafilek, J. Fleig, Impedance spectra of Fe-doped SrTiO3 thin films upon bias voltage: inductive loops as a trace of ion motion, Nanoscale, 8 (2016) 13954-13966.
[35] M. Humayun, L. Xu, L. Zhou, Z. Zheng, Q. Fu, W. Luo, Exceptional co-catalyst free photocatalytic activities of B and Fe co-doped SrTiO3 for CO2 conversion and H2 evolution, Nano Research, 11 (2018) 6391-6404.
[36] D.H. Kim, L. Bi, N.M. Aimon, P. Jiang, G.F. Dionne, C.A. Ross, Combinatorial Pulsed Laser Deposition of Fe, Cr, Mn, and Ni-Substituted SrTiO3 Films on Si Substrates, ACS Combinatorial Science, 14 (2012) 179-190.
[37] J. Shan, F. Raziq, M. Humayun, W. Zhou, Y. Qu, G. Wang, Y. Li, Improved charge separation and surface activation via boron-doped layered polyhedron SrTiO3 for co-catalyst free photocatalytic CO2 conversion, Applied Catalysis B: Environmental, 219 (2017) 10-17.
[38] G. Wang, Y. Ling, H. Wang, X. Yang, C. Wang, J.Z. Zhang, Y. Li, Hydrogen-treated WO3 nanoflakes show enhanced photostability, Energy & Environmental Science, 5 (2012) 6180-6187.
[39] F. Amano, D. Li, B. Ohtani, Fabrication and photoelectrochemical property of tungsten(vi) oxide films with a flake-wall structure, Chemical Communications, 46 (2010) 2769-2771.

[40] J. Su, X. Feng, J.D. Sloppy, L. Guo, C.A. Grimes, Vertically Aligned WO3 Nanowire Arrays Grown Directly on Transparent Conducting Oxide Coated Glass: Synthesis and Photoelectrochemical Properties, Nano Letters, 11 (2011) 203-208.
[41] J. Kim, C.W. Lee, W. Choi, Platinized WO3 as an Environmental Photocatalyst that Generates OH Radicals under Visible Light, Environmental Science & Technology, 44 (2010) 6849-6854.
[42] K.R. Reyes-Gil, C. Wiggenhorn, B.S. Brunschwig, N.S. Lewis, Comparison between the Quantum Yields of Compact and Porous WO3 Photoanodes, The Journal of Physical Chemistry C, 117 (2013) 14947-14957.
[43] X. Zhou, Q. Xu, W. Lei, T. Zhang, X. Qi, G. Liu, K. Deng, J. Yu, Origin of Tunable Photocatalytic Selectivity of Well-Defined α-Fe2O3 Nanocrystals, Small, 10 (2014) 674-679.
[44] S.-W. Cao, Y.-J. Zhu, Hierarchically Nanostructured α-Fe2O3 Hollow Spheres: Preparation, Growth Mechanism, Photocatalytic Property, and Application in Water Treatment, The Journal of Physical Chemistry C, 112 (2008) 6253-6257.
[45] S. Han, L. Hu, Z. Liang, S. Wageh, A.A. Al-Ghamdi, Y. Chen, X. Fang, One-Step Hydrothermal Synthesis of 2D Hexagonal Nanoplates of α-Fe2O3/Graphene Composites with Enhanced Photocatalytic Activity, Advanced Functional Materials, 24 (2014) 5719-5727.
[46] H. Sakamoto, T. Ohara, N. Yasumoto, Y. Shiraishi, S. Ichikawa, S. Tanaka, T. Hirai, Hot-Electron-Induced Highly Efficient O2 Activation by Pt Nanoparticles Supported on Ta2O5 Driven by Visible Light, Journal of the American Chemical Society, 137 (2015) 9324-9332.
[47] A.V. Akimov, R. Asahi, R. Jinnouchi, O.V. Prezhdo, What Makes the Photocatalytic CO2 Reduction on N-Doped Ta2O5 Efficient: Insights from Nonadiabatic Molecular Dynamics, Journal of the American Chemical Society, 137 (2015) 11517-11525.
[48] S. Sato, T. Morikawa, S. Saeki, T. Kajino, T. Motohiro, Visible-Light-Induced Selective CO2 Reduction Utilizing a Ruthenium Complex Electrocatalyst Linked to a p-Type Nitrogen-Doped Ta2O5 Semiconductor, Angewandte Chemie International Edition, 49 (2010) 5101-5105.

[49] N.K. Allam, X.J. Feng, C.A. Grimes, Self-Assembled Fabrication of Vertically Oriented Ta2O5 Nanotube Arrays, and Membranes Thereof, by One-Step Tantalum Anodization, Chemistry of Materials, 20 (2008) 6477-6481.
[50] A. Zhu, Q. Zhao, X. Li, Y. Shi, BiFeO3/TiO2 Nanotube Arrays Composite Electrode: Construction, Characterization, and Enhanced Photoelectrochemical Properties, ACS Applied Materials & Interfaces, 6 (2014) 671-679.
[51] H.-J. Feng, K. Yang, W. Deng, M. Li, M. Wang, B. Duan, F. Liu, J. Tian, X. Guo, The origin of enhanced optical absorption of the BiFeO3/ZnO heterojunction in the visible and terahertz regions, Physical Chemistry Chemical Physics, 17 (2015) 26930-26936.
[52] T. Choi, S. Lee, Y.J. Choi, V. Kiryukhin, S.W. Cheong, Switchable Ferroelectric Diode and Photovoltaic Effect in BiFeO<sub>3</sub&gt, Science, 324 (2009) 63.
[53] F. Gao, X.Y. Chen, K.B. Yin, S. Dong, Z.F. Ren, F. Yuan, T. Yu, Z.G. Zou, J.M. Liu, Visible-Light Photocatalytic Properties of Weak Magnetic BiFeO3 Nanoparticles, Advanced Materials, 19 (2007) 2889-2892.
[54] M. Humayun, A. Zada, Z. Li, M. Xie, X. Zhang, Y. Qu, F. Raziq, L. Jing, Enhanced visible-light activities of porous BiFeO3 by coupling with nanocrystalline TiO2 and mechanism, Applied Catalysis B: Environmental, 180 (2016) 219-226.
[55] M. Xie, Y. Feng, X. Fu, P. Luan, L. Jing, Phosphate-bridged TiO2–BiVO4 nanocomposites with exceptional visible activities for photocatalytic water splitting, Journal of Alloys and Compounds, 631 (2015) 120-124.
[56] S. Sun, W. Wang, L. Zhang, Bi2WO6 Quantum Dots Decorated Reduced Graphene Oxide: Improved Charge Separation and Enhanced Photoconversion Efficiency, The Journal of Physical Chemistry C, 117 (2013) 9113-9120.
[57] X. Ding, K. Zhao, L. Zhang, Enhanced Photocatalytic Removal of Sodium Pentachlorophenate with Self-Doped Bi2WO6 under Visible Light by Generating More Superoxide Ions, Environmental Science & Technology, 48 (2014) 5823-5831.

[58] Z. Zhang, W. Wang, E. Gao, S. Sun, L. Zhang, Photocatalysis Coupled with Thermal Effect Induced by SPR on Ag-Loaded Bi2WO6 with Enhanced Photocatalytic Activity, The Journal of Physical Chemistry C, 116 (2012) 25898-25903.
[59] L. Zhang, Y. Man, Y. Zhu, Effects of Mo Replacement on the Structure and Visible-Light-Induced Photocatalytic Performances of Bi2WO6 Photocatalyst, ACS Catalysis, 1 (2011) 841-848.
[60] W.-C. Huang, L.-M. Lyu, Y.-C. Yang, M.H. Huang, Synthesis of Cu2O Nanocrystals from Cubic to Rhombic Dodecahedral Structures and Their Comparative Photocatalytic Activity, Journal of the American Chemical Society, 134 (2012) 1261-1267.
[61] X. An, K. Li, J. Tang, Cu2O/Reduced Graphene Oxide Composites for the Photocatalytic Conversion of CO2, ChemSusChem, 7 (2014) 1086-1093.
[62] C.W. Li, M.W. Kanan, CO2 Reduction at Low Overpotential on Cu Electrodes Resulting from the Reduction of Thick Cu2O Films, Journal of the American Chemical Society, 134 (2012) 7231-7234.
[63] T. Xiong, W. Cen, Y. Zhang, F. Dong, Bridging the g-C3N4 Interlayers for Enhanced Photocatalysis, ACS Catalysis, 6 (2016) 2462-2472.
[64] X. Bai, L. Wang, R. Zong, Y. Zhu, Photocatalytic Activity Enhanced via g-C3N4 Nanoplates to Nanorods, The Journal of Physical Chemistry C, 117 (2013) 9952-9961.
[65] J. Fu, B. Zhu, C. Jiang, B. Cheng, W. You, J. Yu, Hierarchical Porous O-Doped g-C3N4 with Enhanced Photocatalytic CO2 Reduction Activity, Small, 13 (2017) 1603938.
[66] K. Wang, Q. Li, B. Liu, B. Cheng, W. Ho, J. Yu, Sulfur-doped g-C3N4 with enhanced photocatalytic CO2-reduction performance, Applied Catalysis B: Environmental, 176-177 (2015) 44-52.
[67] W. Xing, W. Tu, Z. Han, Y. Hu, Q. Meng, G. Chen, Template-Induced High-Crystalline g-C3N4 Nanosheets for Enhanced Photocatalytic H2 Evolution, ACS Energy Letters, 3 (2018) 514-519.
[68] A.J. Meier, A. Garg, B. Sutter, J.N. Kuhn, V.R. Bhethanabotla, MoS2 Nanoflowers as a Gateway for Solar-Driven CO2 Photoreduction, ACS Sustainable Chemistry & Engineering, 7 (2019) 265-275.

[69] R.A. Geioushy, S.M. El-Sheikh, I.M. Hegazy, A. Shawky, S. El-Sherbiny, A.-H.T. Kandil, Insights into two-dimensional MoS2 sheets for enhanced CO2 photoreduction to C1 and C2 hydrocarbon products, Materials Research Bulletin, 118 (2019) 110499.
[70] J. Li, Y. Peng, X. Qian, J. Lin, Few-layer Co-doped MoS2 nanosheets with rich active sites as an efficient cocatalyst for photocatalytic H2 production over CdS, Applied Surface Science, 452 (2018) 437-442.
[71] K. Chang, Z. Mei, T. Wang, Q. Kang, S. Ouyang, J. Ye, MoS2/Graphene Cocatalyst for Efficient Photocatalytic H2 Evolution under Visible Light Irradiation, ACS Nano, 8 (2014) 7078-7087.
[72] K. Zhang, M. Fujitsuka, Y. Du, T. Majima, 2D/2D Heterostructured CdS/WS2 with Efficient Charge Separation Improving H2 Evolution under Visible Light Irradiation, ACS Applied Materials & Interfaces, 10 (2018) 20458-20466.
[73] W. Dai, J. Yu, S. Luo, X. Hu, L. Yang, S. Zhang, B. Li, X. Luo, J. Zou, WS2 quantum dots seeding in Bi2S3 nanotubes: A novel Vis-NIR light sensitive photocatalyst with low-resistance junction interface for CO2 reduction, Chemical Engineering Journal, 389 (2020) 123430.
[74] S. Li, Z. Zhao, D. Yu, J.-Z. Zhao, Y. Su, Y. Liu, Y. Lin, W. Liu, H. Xu, Z. Zhang, Few-layer transition metal dichalcogenides (MoS2, WS2, and WSe2) for water splitting and degradation of organic pollutants: Understanding the piezocatalytic effect, Nano Energy, 66 (2019) 104083.
[75] F. Zhang, Y.-H. Li, J.-Y. Li, Z.-R. Tang, Y.-J. Xu, 3D graphene-based gel photocatalysts for environmental pollutants degradation, Environmental Pollution, 253 (2019) 365-376.
[76] Q. Li, B. Guo, J. Yu, J. Ran, B. Zhang, H. Yan, J.R. Gong, Highly Efficient Visible-Light-Driven Photocatalytic Hydrogen Production of CdS-Cluster-Decorated Graphene Nanosheets, Journal of the American Chemical Society, 133 (2011) 10878-10884.
[77] J. Low, J. Yu, W. Ho, Graphene-Based Photocatalysts for CO2 Reduction to Solar Fuel, The Journal of Physical Chemistry Letters, 6 (2015) 4244-4251.
[78] X. Li, J. Yu, S. Wageh, A.A. Al-Ghamdi, J. Xie, Graphene in Photocatalysis: A Review, Small, 12 (2016) 6640-6696.

[79] D. Vairavapandian, P. Vichchulada, M.D. Lay, Preparation and modification of carbon nanotubes: Review of recent advances and applications in catalysis and sensing, Analytica Chimica Acta, 626 (2008) 119-129.
[80] J. Ge, Y. Zhang, S.-J. Park, Recent Advances in Carbonaceous Photocatalysts with Enhanced Photocatalytic Performances: A Mini Review, Materials, 12 (2019).
[81] C. Li, Y. Xu, W. Tu, G. Chen, R. Xu, Metal-free photocatalysts for various applications in energy conversion and environmental purification, Green Chemistry, 19 (2017) 882-899.
[82] A. Léonard, P. Dandoy, E. Danloy, G. Leroux, C.F. Meunier, J.C. Rooke, B.-L. Su, Whole-cell based hybrid materials for green energy production, environmental remediation and smart cell-therapy, Chemical Society Reviews, 40 (2011) 860-885.
[83] N.A. Khan, M. Humayun, M. Usman, Z.A. Ghazi, A. Naeem, A. Khan, A.L. Khan, A.A. Tahir, H. Ullah, Structural Characteristics and Environmental Applications of Covalent Organic Frameworks, Energies, 14 (2021).
[84] M. Usman, M. Ali, B.A. Al-Maythalony, A.S. Ghanem, O.W. Saadi, M. Ali, M.A. Jafar Mazumder, S. Abdel-Azeim, M.A. Habib, Z.H. Yamani, W. Ensinger, Highly Efficient Permeation and Separation of Gases with Metal–Organic Frameworks Confined in Polymeric Nanochannels, ACS Applied Materials & Interfaces, 12 (2020) 49992-50001.
[85] A. Helal, M. Usman, M.E. Arafat, M.M. Abdelnaby, Allyl functionalized UiO-66 metal-organic framework as a catalyst for the synthesis of cyclic carbonates by CO2 cycloaddition, Journal of Industrial and Engineering Chemistry, 89 (2020) 104-110.
[86] A.O. Ibhadon, P. Fitzpatrick, Heterogeneous Photocatalysis: Recent Advances and Applications, Catalysts, 3 (2013).
[87] L. Li, P.A. Salvador, G.S. Rohrer, Photocatalysts with internal electric fields, Nanoscale, 6 (2014) 24-42.
[88] M. Yaseen, M. Humayun, A. Khan, M. Usman, H. Ullah, A.A. Tahir, H. Ullah, Preparation, Functionalization, Modification, and Applications of Nanostructured Gold: A Critical Review, Energies, 14 (2021).

[89] S. Zhu, D. Wang, Photocatalysis: Basic Principles, Diverse Forms of Implementations and Emerging Scientific Opportunities, Advanced Energy Materials, 7 (2017) 1700841.
[90] K.C. Christoforidis, P. Fornasiero, Photocatalysis for Hydrogen Production and CO2 Reduction: The Case of Copper-Catalysts, ChemCatChem, 11 (2019) 368-382.
[91] M. Humayun, M. He, W. Feng, C. Jin, Z. Yao, Y. Wang, W. Pi, S. Ali, A. Khan, M. Wang, Z. Zheng, Q. Fu, H. Xia, W. Luo, Enhanced photocatalytic performance of novel MIL53Sr metal-organic framework (MOF) for RhB dye degradation and H2 evolution by coupling MIL53Fe, Solar Energy, 215 (2021) 121-130.
[92] M. Ashraf, I. Khan, M. Usman, A. Khan, S.S. Shah, A.Z. Khan, K. Saeed, M. Yaseen, M.F. Ehsan, M.N. Tahir, N. Ullah, Hematite and Magnetite Nanostructures for Green and Sustainable Energy Harnessing and Environmental Pollution Control: A Review, Chemical Research in Toxicology, 33 (2020) 1292-1311.
[93] K. Peng, L. Fu, H. Yang, J. Ouyang, Perovskite LaFeO3/montmorillonite nanocomposites: synthesis, interface characteristics and enhanced photocatalytic activity, Scientific Reports, 6 (2016) 19723.
[94] E.A.R. Assirey, Perovskite synthesis, properties and their related biochemical and industrial application, Saudi Pharmaceutical Journal, 27 (2019) 817-829.
[95] N.N. Toan, S. Saukko, V. Lantto, Gas sensing with semiconducting perovskite oxide LaFeO3, Physica B: Condensed Matter, 327 (2003) 279-282.
[96] B. Madhavan, A. Ashok, Review on nanoperovskites: materials, synthesis, and applications for proton and oxide ion conductivity, Ionics, 21 (2015) 601-610.
[97] S. Chen, D. Huang, P. Xu, W. Xue, L. Lei, M. Cheng, R. Wang, X. Liu, R. Deng, Semiconductor-based photocatalysts for photocatalytic and photoelectrochemical water splitting: will we stop with photocorrosion?, Journal of Materials Chemistry A, 8 (2020) 2286-2322.
[98] K. Peng, L. Fu, H. Yang, J. Ouyang, Perovskite LaFeO3/montmorillonite nanocomposites: synthesis, interface characteristics and enhanced photocatalytic activity, Scientific reports, 6 (2016) 19723-19723.

[99] W. Zheng, R. Liu, D. Peng, G. Meng, Hydrothermal synthesis of LaFeO3 under carbonate-containing medium, Materials Letters, 43 (2000) 19-22.
[100] H. Su, L. Jing, K. Shi, C. Yao, H. Fu, Synthesis of large surface area LaFeO3 nanoparticles by SBA-16 template method as high active visible photocatalysts, Journal of Nanoparticle Research, 12 (2010) 967-974.
[101] J. Yu, R. Ran, Y. Zhong, W. Zhou, M. Ni, Z. Shao, Advances in Porous Perovskites: Synthesis and Electrocatalytic Performance in Fuel Cells and Metal–Air Batteries, ENERGY & ENVIRONMENTAL MATERIALS, 3 (2020) 121-145.
[102] H. Wu, R. Hu, T. Zhou, C. Li, W. Meng, J. Yang, A novel efficient boron-doped LaFeO3 photocatalyst with large specific surface area for phenol degradation under simulated sunlight, CrystEngComm, 17 (2015) 3859-3865.
[103] C. Sasikala, N. Durairaj, I. Baskaran, B. Sathyaseelan, M. Henini, E. Manikandan, Transition metal titanium (Ti) doped LaFeO3 nanoparticles for enhanced optical structural and magnetic properties, Journal of Alloys and Compounds, 712 (2017) 870-877.
[104] M. Humayun, Y. Qu, F. Raziq, R. Yan, Z. Li, X. Zhang, L. Jing, Exceptional Visible-Light Activities of TiO2-Coupled N-Doped Porous Perovskite LaFeO3 for 2,4-Dichlorophenol Decomposition and CO2 Conversion, Environmental Science & Technology, 50 (2016) 13600-13610.
[105] M. Humayun, N. Sun, F. Raziq, X. Zhang, R. Yan, Z. Li, Y. Qu, L. Jing, Synthesis of ZnO/Bi-doped porous LaFeO3 nanocomposites as highly efficient nano-photocatalysts dependent on the enhanced utilization of visible-light-excited electrons, Applied Catalysis B: Environmental, 231 (2018) 23-33.
[106] X. Li, H. Lin, X. Chen, H. Niu, J. Liu, T. Zhang, F. Qu, Dendritic α-Fe2O3/TiO2 nanocomposites with improved visible light photocatalytic activity, Physical Chemistry Chemical Physics, 18 (2016) 9176-9185.
[107] P. Luan, M. Xie, D. Liu, X. Fu, L. Jing, Effective charge separation in the rutile TiO2 nanorod-coupled#±-Fe2O3 with exceptionally high visible activities, Scientific Reports, 4 (2014).

[108] R. Huang, R. Liang, H. Fan, S. Ying, L. Wu, X. Wang, G. Yan, Enhanced Photocatalytic Fuel Denitrification over $TiO_2/\alpha\text{-}Fe_2O_3$ Nanocomposites under Visible Light Irradiation, Scientific Reports, 7 (2017) 7858.
[109] M. Xie, X. Fu, L. Jing, P. Luan, Y. Feng, H. Fu, Long-Lived, Visible-Light-Excited Charge Carriers of $TiO_2/BiVO_4$ Nanocomposites and their Unexpected Photoactivity for Water Splitting, Advanced Energy Materials, 4 (2014) 1300995.
[110] X. Fu, M. Xie, P. Luan, L. Jing, Effective visible-excited charge separation in silicate-bridged $ZnO/BiVO_4$ nanocomposite and its contribution to enhanced photocatalytic activity, ACS applied materials & interfaces, 6 21 (2014) 18550-18557.
[111] M. Humayun, Z. Zheng, Q. Fu, W. Luo, Photodegradation of 2,4-dichlorophenol and rhodamine B over n-type ZnO/p-type $BiFeO_3$ heterojunctions: detailed reaction pathway and mechanism, Environmental Science and Pollution Research, 26 (2019) 17696-17706.
[112] N. Sun, Y. Qu, S. Chen, R. Yan, M. Humayun, Y. Liu, L. Bai, L. Jing, H. Fu, Efficient photodecomposition of 2,4-dichlorophenol on recyclable phase-mixed hierarchically structured Bi_2O_3 coupled with phosphate-bridged nano-SnO_2, Environmental Science: Nano, 4 (2017) 1147-1154.
[113] Y. Nosaka, A.Y. Nosaka, Generation and Detection of Reactive Oxygen Species in Photocatalysis, Chem Rev, 117 (2017) 11302-11336.
[114] M. Humayun, H. Ullah, A.A. Tahir, A.R. bin Mohd Yusoff, M.A. Mat Teridi, M.K. Nazeeruddin, W. Luo, An Overview of the Recent Progress in Polymeric Carbon Nitride Based Photocatalysis, The Chemical Record, n/a (2021).
[115] F. Raziq, A. Hayat, M. Humayun, S.K. Baburao Mane, M.B. Faheem, A. Ali, Y. Zhao, S. Han, C. Cai, W. Li, D.-C. Qi, J. Yi, X. Yu, M.B.H. Breese, F. Hassan, F. Ali, A. Mavlonov, K. Dhanabalan, X. Xiang, X. Zu, S. Li, L. Qiao, Photocatalytic solar fuel production and environmental remediation through experimental and DFT based research on CdSe-QDs-coupled P-doped-g-C_3N_4 composites, Applied Catalysis B: Environmental, 270 (2020) 118867.
[116] F. Raziq, J. He, J. Gan, M. Humayun, M.B. Faheem, A. Iqbal, A. Hayat, S. Fazal, J. Yi, Y. Zhao, K. Dhanabalan, X. Wu, A. Mavlonov, T. Ali, F. Hassan, X. Xiang, X. Zu, H.

Shen, S. Li, L. Qiao, Promoting visible-light photocatalytic activities for carbon nitride based 0D/2D/2D hybrid system: Beyond the conventional 4-electron mechanism, Applied Catalysis B: Environmental, 270 (2020) 118870.
[117] A. Albini, M. Fagnoni, 1908: Giacomo Ciamician and the Concept of Green Chemistry, ChemSusChem, 1 (2008) 63-66.
[118] L. Bruner, J. Kozak, Zur Kenntnis der Photokatalyse. I. Die Lichtreaktion in Gemischen: Uransalz + Oxalsäure, Zeitschrift für Elektrochemie und angewandte physikalische Chemie, 17 (1911) 354-360.
[119] N. Serpone, A.V. Emeline, S. Horikoshi, V.N. Kuznetsov, V.K. Ryabchuk, On the genesis of heterogeneous photocatalysis: a brief historical perspective in the period 1910 to the mid-1980s, Photochemical & Photobiological Sciences, 11 (2012) 1121-1150.
[120] S.E. Braslavsky, M.B. Rubin, The history of ozone Part VIII. Photochemical formation of ozone, Photochemical & Photobiological Sciences, 10 (2011) 1515-1520.
[121] C. Belver, J. Bedia, A. Gómez-Avilés, M. Peñas-Garzón, J.J. Rodriguez, Chapter 22 - Semiconductor Photocatalysis for Water Purification, in: S. Thomas, D. Pasquini, S.-Y. Leu, D.A. Gopakumar (Eds.) Nanoscale Materials in Water Purification, Elsevier2019, pp. 581-651.
[122] K. Hashimoto, H. Irie, A. Fujishima, TiO2Photocatalysis: A Historical Overview and Future Prospects, Japanese Journal of Applied Physics, 44 (2005) 8269-8285.
[123] H. Lindquist, Chapter 1 - The Journey of Reinventing the European Electricity Landscape—Challenges and Pioneers, in: L.E. Jones (Ed.) Renewable Energy Integration, Academic Press, Boston, 2014, pp. 3-12.
[124] S.A. Abbasi, N. Abbasi, The likely adverse environmental impacts of renewable energy sources, Applied Energy, 65 (2000) 121-144.
[125] P.J. Boddy, Oxygen Evolution on Semiconducting TiO[sub 2], Journal of The Electrochemical Society, 115 (1968) 199.
[126] M. Kitano, K. Tsujimaru, M. Anpo, Hydrogen Production Using Highly Active Titanium Oxide-based Photocatalysts, Topics in Catalysis, 49 (2008) 4.
[127] G.N. Schrauzer, T.D. Guth, Photolysis of Water and Photoreduction of Nitrogen on Titanium Dioxide, Journal of the American Chemical Society, 99 (1977) 7189-7193.

[128] T. Inoue, A. Fujishima, S. Konishi, K. Honda, Photoelectrocatalytic reduction of carbon dioxide in aqueous suspensions of semiconductor powders, Nature, 277 (1979) 637-638.
[129] F. Fresno, R. Portela, S. Suárez, J.M. Coronado, Photocatalytic materials: recent achievements and near future trends, Journal of Materials Chemistry A, 2 (2014) 2863-2884.
[130] Y. Qu, N. Sun, M. Humayun, A. Zada, Y. Xie, J. Tang, L. Jing, H. Fu, Improved visible-light activities of nanocrystalline CdS by coupling with ultrafine NbN with lattice matching for hydrogen evolution, Sustainable Energy & Fuels, 2 (2018) 549-552.
[131] B. Ohtani, Photocatalysis A to Z—What we know and what we do not know in a scientific sense, Journal of Photochemistry and Photobiology C: Photochemistry Reviews, 11 (2010) 157-178.
[132] X. Yang, D. Wang, Photocatalysis: From Fundamental Principles to Materials and Applications, ACS Applied Energy Materials, 1 (2018) 6657-6693.
[133] C.-y. Wang, R. Pagel, J.K. Dohrmann, D.W. Bahnemann, Antenna mechanism and deaggregation concept: novel mechanistic principles for photocatalysis, Comptes Rendus Chimie, 9 (2006) 761-773.
[134] R. Daghrir, P. Drogui, D. Robert, Modified TiO2 For Environmental Photocatalytic Applications: A Review, Industrial & Engineering Chemistry Research, 52 (2013) 3581-3599.
[135] Z. Zhang, L. Bai, Z. Li, Y. Qu, L. Jing, Review of strategies for the fabrication of heterojunctional nanocomposites as efficient visible-light catalysts by modulating excited electrons with appropriate thermodynamic energy, Journal of Materials Chemistry A, 7 (2019) 10879-10897.
[136] O.K. Dalrymple, E. Stefanakos, M.A. Trotz, D.Y. Goswami, A review of the mechanisms and modeling of photocatalytic disinfection, Applied Catalysis B: Environmental, 98 (2010) 27-38.
[137] K. Wenderich, G. Mul, Methods, Mechanism, and Applications of Photodeposition in Photocatalysis: A Review, Chemical Reviews, 116 (2016) 14587-14619.

[138] M. Usman, M. Humayun, S.S. Shah, H. Ullah, A.A. Tahir, A. Khan, H. Ullah, Bismuth-Graphene Nanohybrids: Synthesis, Reaction Mechanisms, and Photocatalytic Applications—A Review, Energies, 14 (2021).
[139] W. Wang, X. Xu, W. Zhou, Z. Shao, Recent Progress in Metal-Organic Frameworks for Applications in Electrocatalytic and Photocatalytic Water Splitting, Advanced Science, 4 (2017) 1600371.
[140] A. Zada, M. Humayun, F. Raziq, X. Zhang, Y. Qu, L. Bai, C. Qin, L. Jing, H. Fu, Exceptional Visible-Light-Driven Cocatalyst-Free Photocatalytic Activity of g-C3N4 by Well Designed Nanocomposites with Plasmonic Au and SnO2, Advanced Energy Materials, 6 (2016) 1601190.
[141] D. Neena, K.K. Kondamareddy, M. Humayun, V.B. Mohan, D. Lu, D. Fu, W. Gao, Fabrication of ZnO/N-rGO composite as highly efficient visible-light photocatalyst for 2,4-DCP degradation and H2 evolution, Applied Surface Science, 488 (2019) 611-619.
[142] D. Neena, M. Humayun, W. Zuo, C.S. Liu, W. Gao, D.J. Fu, Hierarchical hetero-architectures of in-situ g-C3N4-coupled Fe-doped ZnO micro-flowers with enhanced visible-light photocatalytic activities, Applied Surface Science, 506 (2020) 145017.
[143] N. D, M. Humayun, D. Bhattacharyya, D. Fu, Hierarchical Sr-ZnO/g-C3N4 heterojunction with enhanced photocatalytic activities, Journal of Photochemistry and Photobiology A: Chemistry, 396 (2020) 112515.
[144] F. Raziq, C. Li, M. Humayun, Y. Qu, A. Zada, H. Yu, L. Jing, Synthesis of TiO2/g-C3N4 nanocomposites as efficient photocatalysts dependent on the enhanced photogenerated charge separation, Materials Research Bulletin, 70 (2015) 494-499.
[145] F. Raziq, Y. Qu, X. Zhang, M. Humayun, J. Wu, A. Zada, H. Yu, X. Sun, L. Jing, Enhanced Cocatalyst-Free Visible-Light Activities for Photocatalytic Fuel Production of g-C3N4 by Trapping Holes and Transferring Electrons, The Journal of Physical Chemistry C, 120 (2016) 98-107.
[146] P.V. Kamat, Meeting the Clean Energy Demand: Nanostructure Architectures for Solar Energy Conversion, The Journal of Physical Chemistry C, 111 (2007) 2834-2860.
[147] C.D. Windle, R.N. Perutz, Advances in molecular photocatalytic and electrocatalytic CO2 reduction, Coordination Chemistry Reviews, 256 (2012) 2562-2570.

[148] T. Kothe, S. Pöller, F. Zhao, P. Fortgang, M. Rögner, W. Schuhmann, N. Plumeré, Engineered Electron-Transfer Chain in Photosystem 1 Based Photocathodes Outperforms Electron-Transfer Rates in Natural Photosynthesis, Chemistry – A European Journal, 20 (2014) 11029-11034.

[149] A.W.D. Larkum, Limitations and prospects of natural photosynthesis for bioenergy production, Current Opinion in Biotechnology, 21 (2010) 271-276.

[150] J. Barber, Photosynthetic energy conversion: natural and artificial, Chemical Society Reviews, 38 (2009) 185-196.

[151] M.-Q. Yang, N. Zhang, M. Pagliaro, Y.-J. Xu, Artificial photosynthesis over graphene–semiconductor composites. Are we getting better?, Chemical Society Reviews, 43 (2014) 8240-8254.

[152] K. Xie, N. Umezawa, N. Zhang, P. Reunchan, Y. Zhang, J. Ye, Self-doped SrTiO3−δ photocatalyst with enhanced activity for artificial photosynthesis under visible light, Energy & Environmental Science, 4 (2011) 4211-4219.

[153] F. Raziq, M. Humayun, A. Ali, T. Wang, A. Khan, Q. Fu, W. Luo, H. Zeng, Z. Zheng, B. Khan, H. Shen, X. Zu, S. Li, L. Qiao, Synthesis of S-Doped porous g-C3N4 by using ionic liquids and subsequently coupled with Au-TiO2 for exceptional cocatalyst-free visible-light catalytic activities, Applied Catalysis B: Environmental, 237 (2018) 1082-1090.

[154] J. Low, B. Cheng, J. Yu, Surface modification and enhanced photocatalytic CO2 reduction performance of TiO2: a review, Applied Surface Science, 392 (2017) 658-686.

[155] J. Fu, J. Yu, C. Jiang, B. Cheng, g-C3N4-Based Heterostructured Photocatalysts, Advanced Energy Materials, 8 (2018) 1701503.

[156] J. Wu, Y. Huang, W. Ye, Y. Li, CO2 Reduction: From the Electrochemical to Photochemical Approach, Advanced Science, 4 (2017) 1700194.

[157] F. Raziq, L. Sun, Y. Wang, X. Zhang, M. Humayun, S. Ali, L. Bai, Y. Qu, H. Yu, L. Jing, Synthesis of Large Surface-Area g-C3N4 Comodified with MnOx and Au-TiO2 as Efficient Visible-Light Photocatalysts for Fuel Production, Advanced Energy Materials, 8 (2018) 1701580.

[158] G. Liu, N. Hoivik, K. Wang, H. Jakobsen, Engineering TiO_2 nanomaterials for CO_2 conversion/solar fuels, Solar Energy Materials and Solar Cells, 105 (2012) 53-68.

[159] K. Li, X. An, K.H. Park, M. Khraisheh, J. Tang, A critical review of CO_2 photoconversion: Catalysts and reactors, Catalysis Today, 224 (2014) 3-12.

[160] M. Humayun, Q. Fu, Z. Zheng, H. Li, W. Luo, Improved visible-light catalytic activities of novel Au/P-doped g-C_3N_4 photocatalyst for solar fuel production and mechanism, Applied Catalysis A: General, 568 (2018) 139-147.

[161] S. Chen, R. Yan, X. Zhang, K. Hu, Z. Li, M. Humayun, Y. Qu, L. Jing, Photogenerated electron modulation to dominantly induce efficient 2,4-dichlorophenol degradation on BiOBr nanoplates with different phosphate modification, Applied Catalysis B: Environmental, 209 (2017) 320-328.

[162] M. Humayun, Z. Hu, A. Khan, W. Cheng, Y. Yuan, Z. Zheng, Q. Fu, W. Luo, Highly efficient degradation of 2,4-dichlorophenol over CeO_2/g-C_3N_4 composites under visible-light irradiation: Detailed reaction pathway and mechanism, Journal of Hazardous Materials, 364 (2019) 635-644.

[163] I. Ullah, F. Ali, Z. Ali, M. Humayun, Z.U. wahab, Glycol stabilized magnetic nanoparticles for photocatalytic degradation of xylenol orange, Materials Research Express, 5 (2018) 055509.

[164] X. Zhao, J. Zhang, B. Wang, A. Zada, M. Humayun, Biochemical Synthesis of Ag/AgCl Nanoparticles for Visible-Light-Driven Photocatalytic Removal of Colored Dyes, Materials, 8 (2015).

[165] J. Ma, F. Wang, M. Mostafavi, Ultrafast Chemistry of Water Radical Cation, $H_2O^{\bullet+}$, in Aqueous Solutions, Molecules, 23 (2018).

[166] M.D. Hernández-Alonso, F. Fresno, S. Suárez, J.M. Coronado, Development of alternative photocatalysts to TiO_2: Challenges and opportunities, Energy & Environmental Science, 2 (2009) 1231-1257.

[167] S. Ali, M. Humayun, W. Pi, Y. Yuan, M. Wang, A. Khan, P. Yue, L. Shu, Z. Zheng, Q. Fu, W. Luo, Fabrication of $BiFeO_3$-g-C_3N_4-WO_3 Z-scheme heterojunction as highly efficient visible-light photocatalyst for water reduction and 2,4-dichlorophenol degradation: Insight mechanism, Journal of Hazardous Materials, 397 (2020) 122708.

[168] K. Maeda, K. Domen, New Non-Oxide Photocatalysts Designed for Overall Water Splitting under Visible Light, The Journal of Physical Chemistry C, 111 (2007) 7851-7861.
[169] G.C. Mather, M.S. Islam, F.M. Figueiredo, Atomistic Study of a CaTiO3-Based Mixed Conductor: Defects, Nanoscale Clusters, and Oxide-Ion Migration, Advanced Functional Materials, 17 (2007) 905-912.
[170] S. Mtougui, R. Khalladi, S. Ziti, H. Labrim, L. Bahmad, Magnetic properties of the perovskite BiFeO3: Monte Carlo simulation, Superlattices and Microstructures, 123 (2018) 111-118.
[171] E.A. Katz, Perovskite: Name Puzzle and German-Russian Odyssey of Discovery, Helvetica Chimica Acta, 103 (2020) e2000061.
[172] L. Abbes, H. Noura, Perovskite oxides MRuO3 (M=Sr, Ca and Ba): Structural distortion, electronic and magnetic properties with GGA and GGA-modified Becke–Johnson approaches, Results in Physics, 5 (2015) 38-52.
[173] P. Goel, S. Sundriyal, V. Shrivastav, S. Mishra, D.P. Dubal, K.-H. Kim, A. Deep, Perovskite materials as superior and powerful platforms for energy conversion and storage applications, Nano Energy, 80 (2021) 105552.
[174] S. Gupta, W. Kellogg, H. Xu, X. Liu, J. Cho, G. Wu, Bifunctional Perovskite Oxide Catalysts for Oxygen Reduction and Evolution in Alkaline Media, Chemistry – An Asian Journal, 11 (2016) 10-21.
[175] Y. Zhang, H.-Y. Ye, W. Zhang, R.-G. Xiong, Room-temperature ABX3-typed molecular ferroelectric: [C5H9–NH3][CdCl3], Inorganic Chemistry Frontiers, 1 (2014) 118-123.
[176] W. Si, Y. Wang, Y. Peng, J. Li, Selective Dissolution of A-Site Cations in ABO3 Perovskites: A New Path to High-Performance Catalysts, Angewandte Chemie International Edition, 54 (2015) 7954-7957.
[177] V.M. Zainullina, M.A. Korotin, V.L. Kozhevnikov, Electronic properties of disordered perovskite-like ferrites: Coherent potential approach, Progress in Solid State Chemistry, 60 (2020) 100284.

[178] K.K. Bamzai, M. Bhat, Electrical and Magnetic Properties of Some Rare Earth Orthoferrites (RFeO3 where R = Y, Ho, Er) Systems, Integrated Ferroelectrics, 158 (2014) 108-122.
[179] T. Yamaguchi, Theory of spin reorientation in rare-earth orthochromites and orthoferrites, Journal of Physics and Chemistry of Solids, 35 (1974) 479-500.
[180] S. Yuan, Y. Wang, M. Shao, F. Chang, B. Kang, Y. Isikawa, S. Cao, Magnetic properties of NdFeO3 single crystal in the spin reorientation region, Journal of Applied Physics, 109 (2011) 07E141.
[181] R.M. White, R.J. Nemanich, C. Herring, Light scattering from magnetic excitations in orthoferrites, Physical Review B, 25 (1982) 1822-1836.
[182] S.N. Tijare, M.V. Joshi, P.S. Padole, P.A. Mangrulkar, S.S. Rayalu, N.K. Labhsetwar, Photocatalytic hydrogen generation through water splitting on nano-crystalline LaFeO3 perovskite, International Journal of Hydrogen Energy, 37 (2012) 10451-10456.
[183] K.J. May, D.P. Fenning, T. Ming, W.T. Hong, D. Lee, K.A. Stoerzinger, M.D. Biegalski, A.M. Kolpak, Y. Shao-Horn, Thickness-Dependent Photoelectrochemical Water Splitting on Ultrathin LaFeO3 Films Grown on Nb:SrTiO3, The Journal of Physical Chemistry Letters, 6 (2015) 977-985.
[184] L.M. Misch, A. Birkel, C.A. Figg, B.P. Fors, C.J. Hawker, G.D. Stucky, R. Seshadri, Rapid microwave-assisted sol-gel preparation of Pd-substituted LnFeO3 (Ln = Y, La): phase formation and catalytic activity, Dalton transactions, 43 5 (2014) 2079-2087.
[185] C.A.L. Dixon, C.M. Kavanagh, K.S. Knight, W. Kockelmann, F.D. Morrison, P. Lightfoot, Thermal evolution of the crystal structure of the orthorhombic perovskite LaFeO3, Journal of Solid State Chemistry, 230 (2015) 337-342.
[186] M. Shandilya, R. Rai, J. Singh, Review: hydrothermal technology for smart materials, Advances in Applied Ceramics, 115 (2016) 354-376.
[187] S. Thirumalairajan, K. Girija, I. Ganesh, D. Mangalaraj, C. Viswanathan, A. Balamurugan, N. Ponpandian, Controlled synthesis of perovskite LaFeO3 microsphere

composed of nanoparticles via self-assembly process and their associated photocatalytic activity, Chemical Engineering Journal, 209 (2012) 420-428.
[188] R. Dhinesh Kumar, R. Jayavel, Facile hydrothermal synthesis and characterization of LaFeO3 nanospheres for visible light photocatalytic applications, Journal of Materials Science: Materials in Electronics, 25 (2014) 3953-3961.
[189] T.T.N. Phan, A.N. Nikoloski, P.A. Bahri, D. Li, Optimizing photocatalytic performance of hydrothermally synthesized LaFeO3 by tuning material properties and operating conditions, Journal of Environmental Chemical Engineering, 6 (2018) 1209-1218.
[190] S. Thirumalairajan, K. Girija, V.R. Mastelaro, N. Ponpandian, Photocatalytic degradation of organic dyes under visible light irradiation by floral-like LaFeO3 nanostructures comprised of nanosheet petals, New Journal of Chemistry, 38 (2014) 5480-5490.
[191] G. Demazeau, Solvothermal reactions: an original route for the synthesis of novel materials, Journal of Materials Science, 43 (2008) 2104-2114.
[192] H. Kominami, H. Inoue, S. Konishi, Y. Kera, Synthesis of Perovskite-Type Lanthanum Iron Oxide by Glycothermal Reaction of a Lanthanum–Iron Precursor, Journal of the American Ceramic Society, 85 (2002) 2148-2150.
[193] S. Esposito, "Traditional" Sol-Gel Chemistry as a Powerful Tool for the Preparation of Supported Metal and Metal Oxide Catalysts, Materials, 12 (2019).
[194] S. Li, L. Jing, W. Fu, L. Yang, B. Xin, H. Fu, Photoinduced charge property of nanosized perovskite-type LaFeO3 and its relationships with photocatalytic activity under visible irradiation, Materials Research Bulletin, 42 (2007) 203-212.
[195] M. Ismael, M. Wark, Perovskite-type LaFeO3: Photoelectrochemical Properties and Photocatalytic Degradation of Organic Pollutants Under Visible Light Irradiation, Catalysts, 9 (2019).
[196] W. Azouzi, W. Sigle, H. Labrim, M. Benaissa, Sol-gel synthesis of nanoporous LaFeO3 powders for solar applications, Materials Science in Semiconductor Processing, 104 (2019) 104682.

[197] Q. Feng, J. Zhou, W. Luo, L. Ding, W. Cai, Photo-Fenton removal of tetracycline hydrochloride using LaFeO3 as a persulfate activator under visible light, Ecotoxicology and Environmental Safety, 198 (2020) 110661.

[198] K.M. Parida, K.H. Reddy, S. Martha, D.P. Das, N. Biswal, Fabrication of nanocrystalline LaFeO3: An efficient sol–gel auto-combustion assisted visible light responsive photocatalyst for water decomposition, International Journal of Hydrogen Energy, 35 (2010) 12161-12168.

[199] Y. Rao, Y. Zhang, F. Han, H. Guo, Y. Huang, R. Li, F. Qi, J. Ma, Heterogeneous activation of peroxymonosulfate by LaFeO3 for diclofenac degradation: DFT-assisted mechanistic study and degradation pathways, Chemical Engineering Journal, 352 (2018) 601-611.

[200] I. Bilecka, M. Niederberger, Microwave chemistry for inorganic nanomaterials synthesis, Nanoscale, 2 (2010) 1358-1374.

[201] S. Farhadi, Z. Momeni, M. Taherimehr, Rapid synthesis of perovskite-type LaFeO3 nanoparticles by microwave-assisted decomposition of bimetallic La[Fe(CN)6]·5H2O compound, Journal of Alloys and Compounds, 471 (2009) L5-L8.

[202] P. Tang, Y. Tong, H. Chen, F. Cao, G. Pan, Microwave-assisted synthesis of nanoparticulate perovskite LaFeO3 as a high active visible-light photocatalyst, Current Applied Physics, 13 (2013) 340-343.

[203] E.M. Kostyukhin, A.L. Kustov, L.M. Kustov, One-step hydrothermal microwave-assisted synthesis of LaFeO3 nanoparticles, Ceramics International, 45 (2019) 14384-14388.

[204] V.M. Gaikwad, J.R. Sheikh, S.A. Acharya, Investigation of photocatalytic and dielectric behavior of LaFeO3 nanoparticles prepared by microwave-assisted sol–gel combustion route, Journal of Sol-Gel Science and Technology, 76 (2015) 27-35.

[205] S.S. Jamali, D. Singh, H. Tavakkoli, F. Kaveh, T. Tabari, Microwave-assisted synthesis of nanostructured perovskite-type oxide with efficient photocatalytic activity against organic reactants in gaseous and aqueous phases, Materials Science in Semiconductor Processing, 64 (2017) 47-54.

[206] H. Xu, B.W. Zeiger, K.S. Suslick, Sonochemical synthesis of nanomaterials, Chemical Society Reviews, 42 (2013) 2555-2567.
[207] P. Mehdizadeh, O. Amiri, S. Rashki, M. Salavati-Niasari, M. Salimian, L.K. Foong, Effective removal of organic pollution by using sonochemical prepared LaFeO3 perovskite under visible light, Ultrasonics Sonochemistry, 61 (2020) 104848.
[208] P. Kanhere, Z. Chen, A Review on Visible Light Active Perovskite-Based Photocatalysts, Molecules, 19 (2014).
[209] S. Li, Y. Li, Y. Chen, L. Xu, Q. Chen, Y. Qu, G. Wang, P. Zhu, D. Wang, W. Qin, Enhanced Visible-Light Photoactivities of Perovskite-Type LaFeO3 Nanocrystals by Simultaneously Doping Er3+ and Coupling MgO for CO2 Reduction, ChemCatChem, 12 (2020) 623-630.
[210] B.R.A. Nijboer, On the theory of electronic semiconductors, Proceedings of the Physical Society, 51 (1939) 575-584.
[211] A.H. Wilson, P.A.M. Dirac, The theory of electronic semi-conductors, Proceedings of the Royal Society of London. Series A, Containing Papers of a Mathematical and Physical Character, 133 (1931) 458-491.
[212] W. Mönch, Semiconductor Surfaces and Interfaces, Springer Berlin Heidelberg2013.
[213] C.A. Hogarth, The transistor-its invention and its current prospects, Physics in Technology, 4 (1973) 173-186.
[214] S. Lany, Semiconducting transition metal oxides, Journal of Physics: Condensed Matter, 27 (2015) 283203.
[215] W. Shockley, The Theory of p-n Junctions in Semiconductors and p-n Junction Transistors, Bell System Technical Journal, 28 (1949) 435-489.
[216] R.D. Dupuis, M.R. Krames, History, Development, and Applications of High-Brightness Visible Light-Emitting Diodes, J. Lightwave Technol., 26 (2008) 1154-1171.
[217] J. Zhang, K. Tse, M. Wong, Y. Zhang, J. Zhu, A brief review of co-doping, Frontiers of Physics, 11 (2016) 117405.

[218] L. Xu, S. Yuan, H. Zeng, J. Song, A comprehensive review of doping in perovskite nanocrystals/quantum dots: evolution of structure, electronics, optics, and light-emitting diodes, Materials Today Nano, 6 (2019) 100036.

[219] R. Maity, M.S. Sheikh, A. Dutta, T.P. Sinha, Visible Light Driven Photocatalytic Activity of Granular Pr Doped LaFeO3, Journal of Electronic Materials, 48 (2019) 4856-4865.

[220] M. Dhiman, S. Singhal, Effect of doping of different rare earth (europium, gadolinium, dysprosium and neodymium) metal ions on structural, optical and photocatalytic properties of LaFeO3 perovskites, Journal of Rare Earths, 37 (2019) 1279-1287.

[221] Z. Zhong, K. Chen, Y. Ji, Q. Yan, Methane combustion over B-site partially substituted perovskite-type LaFeO3 prepared by sol-gel method, Applied Catalysis A: General, 156 (1997) 29-41.

[222] G. Wang, C. Cheng, J. Zhu, L. Wang, S. Gao, X. Xia, Enhanced degradation of atrazine by nanoscale LaFe1-xCuxO3-δ perovskite activated peroxymonosulfate: Performance and mechanism, Science of The Total Environment, 673 (2019) 565-575.

[223] T.T.N. Phan, A.N. Nikoloski, P.A. Bahri, D. Li, Heterogeneous photo-Fenton degradation of organics using highly efficient Cu-doped LaFeO3 under visible light, Journal of Industrial and Engineering Chemistry, 61 (2018) 53-64.

[224] K. Pan, C. Yang, J. Hu, W. Yang, B. Liu, J. Yang, S. Liang, K. Xiao, H. Hou, Oxygen vacancy mediated surface charge redistribution of Cu-substituted LaFeO3 for degradation of bisphenol A by efficient decomposition of H2O2, Journal of Hazardous Materials, 389 (2020) 122072.

[225] L. Hou, G. Sun, K. Liu, Y. Li, F. Gao, Preparation, characterization and investigation of catalytic activity of Li-doped LaFeO3 nanoparticles, Journal of Sol-Gel Science and Technology, 40 (2006) 9-14.

[226] G. Iervolino, V. Vaiano, D. Sannino, L. Rizzo, V. Palma, Enhanced photocatalytic hydrogen production from glucose aqueous matrices on Ru-doped LaFeO3, Applied Catalysis B: Environmental, 207 (2017) 182-194.

[227] F.-t. Li, Y. Liu, R.-h. Liu, Z.-m. Sun, D.-s. Zhao, C.-g. Kou, Preparation of Ca-doped LaFeO3 nanopowders in a reverse microemulsion and their visible light photocatalytic activity, Materials Letters, 64 (2010) 223-225.

[228] P. Garcia-Muñoz, F. Fresno, C. Lefevre, D. Robert, N. Keller, Synergy effect between photocatalysis and heterogeneous photo-Fenton catalysis on Ti-doped LaFeO3 perovskite for high efficiency light-assisted water treatment, Catalysis Science & Technology, 10 (2020) 1299-1310.

[229] C. Cheng, S. Gao, J. Zhu, G. Wang, L. Wang, X. Xia, Enhanced performance of LaFeO3 perovskite for peroxymonosulfate activation through strontium doping towards 2,4-D degradation, Chemical Engineering Journal, 384 (2020) 123377.

[230] P. Garcia-Muñoz, C. Lefevre, D. Robert, N. Keller, Ti-substituted LaFeO3 perovskite as photoassisted CWPO catalyst for water treatment, Applied Catalysis B: Environmental, 248 (2019) 120-128.

[231] T. Vijayaraghavan, M. Bradha, P. Babu, K.M. Parida, G. Ramadoss, S. Vadivel, R. Selvakumar, A. Ashok, Influence of secondary oxide phases in enhancing the photocatalytic properties of alkaline earth elements doped LaFeO3 nanocomposites, Journal of Physics and Chemistry of Solids, 140 (2020) 109377.

[232] S. Dong, K. Xu, G. Tian, Photocatalytic activities of LaFe1−xZnxO3 nanocrystals prepared by sol–gel auto-combustion method, Journal of Materials Science, 44 (2009) 2548-2552.

[233] P. Garcia-Muñoz, F. Fresno, C. Lefevre, D. Robert, N. Keller, Highly robust La1-xTixFeO3 dual catalyst with combined photocatalytic and photo-CWPO activity under visible light for 4-chlorophenol removal in water, Applied Catalysis B: Environmental, 262 (2020) 118310.

[234] H. Ullah, A.A. Tahir, S. Bibi, T.K. Mallick, S.Z. Karazhanov, Electronic properties of β-TaON and its surfaces for solar water splitting, Applied Catalysis B: Environmental, 229 (2018) 24-31.

[235] Z. Zheng, X. Zu, Y. Zhang, W. Zhou, Rational design of type-II nano-heterojunctions for nanoscale optoelectronics, Materials Today Physics, 15 (2020) 100262.

[236] J. Low, C. Jiang, B. Cheng, S. Wageh, A.A. Al-Ghamdi, J. Yu, A Review of Direct Z-Scheme Photocatalysts, Small Methods, 1 (2017) 1700080.
[237] Y. Ye, H. Yang, H. Zhang, J. Jiang, A promising Ag2CrO4/LaFeO3 heterojunction photocatalyst applied to photo-Fenton degradation of RhB, Environmental Technology, 41 (2020) 1486-1503.
[238] Y. Ye, H. Yang, R. Li, X. Wang, Enhanced photocatalytic performance and mechanism of Ag-decorated LaFeO3 nanoparticles, Journal of Sol-Gel Science and Technology, 82 (2017) 509-518.
[239] S. Guan, R. Li, X. Sun, T. Xian, H. Yang, Construction of novel ternary Au/LaFeO3/Cu2O composite photocatalysts for RhB degradation via photo-Fenton catalysis, Materials Technology, (2020) 1-13.
[240] A.-A. Hoseini, S. Farhadi, A. Zabardasti, F. Siadatnasab, A novel n-type CdS nanorods/p-type LaFeO3 heterojunction nanocomposite with enhanced visible-light photocatalytic performance, RSC Advances, 9 (2019) 24489-24504.
[241] S. Acharya, D. Kandi, K. Parida, CdS QD Decorated LaFeO3 Nanosheets for Photocatalytic Application Under Visible Light Irradiation, ChemistrySelect, 5 (2020) 6153-6161.
[242] K. Wang, H. Niu, J. Chen, J. Song, C. Mao, S. Zhang, S. Zheng, B. Liu, C. Chen, Facile Synthesis of CeO_2-$LaFeO_3$ Perovskite Composite and Its Application for 4-(Methylnitrosamino)-1-(3-Pyridyl)-1-Butanone (NNK) Degradation, Materials (Basel), 2016.
[243] Y. Soltanabadi, M. Jourshabani, Z. Shariatinia, Synthesis of novel CuO/LaFeO3 nanocomposite photocatalysts with superior Fenton-like and visible light photocatalytic activities for degradation of aqueous organic contaminants, Separation and Purification Technology, 202 (2018) 227-241.
[244] Y. Liu, M. Wu, L. Ren, C. Wang, Z. Li, L. Ling, Y. Guo, Heterogeneous Photo-Fenton Catalytic Oxidation of Ciprofloxacin Using LaFeO3/Diatomite Composite Photocatalysts under Visible Light, ChemistrySelect, 5 (2020) 14792-14799.
[245] M. Sukumar, L.J. Kennedy, J.J. Vijaya, B. Al-Najar, M. Bououdina, Facile synthesis of Fe3+ doped La2CuO4/LaFeO3 perovskite nanocomposites: Structural,

optical, magnetic and catalytic properties, Materials Science in Semiconductor Processing, 100 (2019) 225-235.

[246] D. Zhang, M. Chen, H. Zou, Y. Zhang, J. Hu, H. Wang, B. Zi, J. Zhang, Z. Zhu, L. Duan, Q. Liu, Microwave-assisted synthesis of porous and hollow α-Fe2O3/LaFeO3 nanostructures for acetone gas sensing as well as photocatalytic degradation of methylene blue, Nanotechnology, 31 (2020) 215601.

[247] B.M. Pirzada, Pushpendra, R.K. Kunchala, B.S. Naidu, Synthesis of LaFeO3/Ag2CO3 Nanocomposites for Photocatalytic Degradation of Rhodamine B and p-Chlorophenol under Natural Sunlight, ACS Omega, 4 (2019) 2618-2629.

[248] S. Manchala, A. Gandamalla, N.R. Vempuluru, S. Muthukonda Venkatakrishnan, V. Shanker, High potential and robust ternary LaFeO3/CdS/carbon quantum dots nanocomposite for photocatalytic H2 evolution under sunlight illumination, Journal of Colloid and Interface Science, 583 (2021) 255-266.

[249] L. Jin, X. Zhou, X. Ning, L. Zhan, M. Kong, K. Tan, J. Li, Z. Lin, Boosting visible light photocatalytic performance of g-C3N4 nanosheets by combining with LaFeO3 nanoparticles, Materials Research Bulletin, 102 (2018) 353-361.

[250] S. Acharya, S. Mansingh, K.M. Parida, The enhanced photocatalytic activity of g-C3N4-LaFeO3 for the water reduction reaction through a mediator free Z-scheme mechanism, Inorganic Chemistry Frontiers, 4 (2017) 1022-1032.

[251] K. Xu, X. Yang, L. Ruan, S. Qi, J. Liu, K. Liu, S. Pan, G. Feng, Z. Dai, X. Yang, R. Li, J. Feng, Superior Adsorption and Photocatalytic Degradation Capability of Mesoporous LaFeO3/g-C3N4 for Removal of Oxytetracycline, Catalysts, 10 (2020).

[252] T. Vijayaraghavan, R. Althaf, P. Babu, K.M. Parida, S. Vadivel, A.M. Ashok, Visible light active LaFeO3 nano perovskite-RGO-NiO composite for efficient H2 evolution by photocatalytic water splitting and textile dye degradation, Journal of Environmental Chemical Engineering, 9 (2021) 104675.

[253] S. Acharya, D.K. Padhi, K.M. Parida, Visible light driven LaFeO3 nano sphere/RGO composite photocatalysts for efficient water decomposition reaction, Catalysis Today, (2017).

[254] X. Ren, H. Yang, S. Gen, J. Zhou, T. Yang, X. Zhang, Z. Cheng, S. Sun, Controlled growth of LaFeO3 nanoparticles on reduced graphene oxide for highly efficient photocatalysis, Nanoscale, 8 (2016) 752-756.

[255] H. Sabeeh, S. Musaddiq, M. Shahid, M.A. Khan, M. Sher, M.F. Warsi, Rare earth substituted nanocrystalline LaFeO3 perovskites and their composites with reduced graphene oxide for enhanced photocatalytic and other potential applications, Materials Research Express, 5 (2018) 065062.

[256] Y. Song, S. Xue, G. Wang, J. Jin, Q. Liang, Z. Li, S. Xu, Enhanced photocatalytic decomposition of an organic dye under visible light with a stable LaFeO3/AgBr heterostructured photocatalyst, Journal of Physics and Chemistry of Solids, 121 (2018) 329-338.

[257] J. Xu, C. Liu, J. Niu, Y. Zhu, B. Zang, M. Xie, M. Chen, Synthesis of LaFeO3/Bi3NbO7 p-n heterojunction photocatalysts with enhanced visible-light-responsive activity for photocatalytic reduction of Cr(Ⅵ), Journal of Alloys and Compounds, 815 (2020) 152492.

[258] K. Xu, J. Feng, Superior photocatalytic performance of LaFeO3/g-C3N4 heterojunction nanocomposites under visible light irradiation, RSC Advances, 7 (2017) 45369-45376.

[259] M. Ismael, Y. Wu, A facile synthesis method for fabrication of LaFeO3/g-C3N4 nanocomposite as efficient visible-light-driven photocatalyst for photodegradation of RhB and 4-CP, New Journal of Chemistry, 43 (2019) 13783-13793.

[260] Q. Zhang, Y. Huang, S. Peng, Y. Zhang, Z. Shen, J.-j. Cao, W. Ho, S.C. Lee, D.Y.H. Pui, Perovskite LaFeO3-SrTiO3 composite for synergistically enhanced NO removal under visible light excitation, Applied Catalysis B: Environmental, 204 (2017) 346-357.

[261] W. Gao, C. Zhang, S. Cui, Q. Liang, S. Xu, Z. Li, In situ Synthesis of p–n LaFeO3/ZnIn2S4 Heterojunctions for Enhanced Photocatalytic Activity, Nano, 14 (2019) 1950096.

[262] P. Garcia-Muñoz, F. Fresno, J. Ivanez, D. Robert, N. Keller, Activity enhancement pathways in LaFeO3@TiO2 heterojunction photocatalysts for visible and solar light

driven degradation of myclobutanil pesticide in water, Journal of Hazardous Materials, 400 (2020) 123099.
[263] C. Gong, Z. Zhang, S. Lin, Z. Wu, L. Sun, C. Ye, Y. Hu, C. Lin, Electrochemical synthesis of perovskite LaFeO3 nanoparticle-modified TiO2 nanotube arrays for enhanced visible-light photocatalytic activity, New Journal of Chemistry, 43 (2019) 16506-16514.
[264] R. Dhinesh Kumar, R. Thangappan, R. Jayavel, Synthesis and characterization of LaFeO3/TiO2 nanocomposites for visible light photocatalytic activity, Journal of Physics and Chemistry of Solids, 101 (2017) 25-33.
[265] S. Acharya, G. Swain, K.M. Parida, MoS2-mesoporous LaFeO3 hybrid photocatalyst: Highly efficient visible-light driven photocatalyst, International Journal of Hydrogen Energy, 45 (2020) 11502-11511.
[266] K. Xu, H. Xu, G. Feng, J. Feng, Photocatalytic hydrogen evolution performance of NiS cocatalyst modified LaFeO3/g-C3N4 heterojunctions, New Journal of Chemistry, 41 (2017) 14602-14609.
[267] X.-T. Wang, Y. Li, X.-Q. Zhang, J.-F. Li, X. Li, C.-W. Wang, Design and fabrication of NiS/LaFeO3 heterostructures for high efficient photodegradation of organic dyes, Applied Surface Science, 504 (2020) 144363.
[268] G. Iervolino, V. Vaiano, D. Sannino, L. Rizzo, A. Galluzzi, M. Polichetti, G. Pepe, P. Campiglia, Hydrogen production from glucose degradation in water and wastewater treated by Ru-LaFeO3/Fe2O3 magnetic particles photocatalysis and heterogeneous photo-Fenton, International Journal of Hydrogen Energy, 43 (2018) 2184-2196.
[269] S. Guan, H. Yang, X. Sun, T. Xian, Preparation and promising application of novel LaFeO3/BiOBr heterojunction photocatalysts for photocatalytic and photo-Fenton removal of dyes, Optical Materials, 100 (2020) 109644.
[270] Y. Wu, H. Wang, W. Tu, Y. Liu, Y.Z. Tan, X. Yuan, J.W. Chew, Quasi-polymeric construction of stable perovskite-type LaFeO3/g-C3N4 heterostructured photocatalyst for improved Z-scheme photocatalytic activity via solid p-n heterojunction interfacial effect, Journal of Hazardous Materials, 347 (2018) 412-422.

[271] X. Gao, Y. Shang, L. Liu, W. Nie, A plasmonic Z-scheme three-component photocatalyst g-C3N4/Ag/LaFeO3 with enhanced visible-light photocatalytic activities, Optical Materials, 88 (2019) 229-237.
[272] T. Lv, H. Wang, W. Hong, P. Wang, L. Jia, In situ self-assembly synthesis of sandwich-like TiO2/reduced graphene oxide/LaFeO3 Z-scheme ternary heterostructure towards enhanced photocatalytic hydrogen production, Molecular Catalysis, 475 (2019) 110497.
[273] I. Khan, N. Sun, Y. Wang, Z. Li, Y. Qu, L. Jing, Synthesis of SnO2/yolk-shell LaFeO3 nanocomposites as efficient visible-light photocatalysts for 2,4-dichlorophenol degradation, Materials Research Bulletin, 127 (2020) 110857.
[274] K. Gao, S. Li, Multi-modal TiO2–LaFeO3 composite films with high photocatalytic activity and hydrophilicity, Applied Surface Science, 258 (2012) 6460-6464.
[275] S. Acharya, K. Parida, A Visible Light-Driven Zn/Cr–LaFeO3 Nanocomposite with Enhanced Photocatalytic Activity towards H2 Production and RhB Degradation, ChemistrySelect, 2 (2017) 10239-10248.
[276] Y. Ye, H. Yang, X. Wang, W. Feng, Photocatalytic, Fenton and photo-Fenton degradation of RhB over Z-scheme g-C3N4/LaFeO3 heterojunction photocatalysts, Materials Science in Semiconductor Processing, 82 (2018) 14-24.
[277] J. Luo, R. Li, Y. Chen, X. Zhou, X. Ning, L. Zhan, L. Ma, X. Xu, L. Xu, L. Zhang, Rational design of Z-scheme LaFeO3/SnS2 hybrid with boosted visible light photocatalytic activity towards tetracycline degradation, Separation and Purification Technology, 210 (2019) 417-430.
[278] M. Humayun, Z. Li, L. Sun, X. Zhang, F. Raziq, A. Zada, Y. Qu, L. Jing, Coupling of Nanocrystalline Anatase TiO2 to Porous Nanosized LaFeO3 for Efficient Visible-Light Photocatalytic Degradation of Pollutants, Nanomaterials, 6 (2016).
[279] L. Jing, Y. Qu, H. Su, C. Yao, H. Fu, Synthesis of High-Activity TiO2-Based Photocatalysts by Compounding a Small Amount of Porous Nanosized LaFeO3 and the Activity-Enhanced Mechanisms, The Journal of Physical Chemistry C, 115 (2011) 12375-12380.

[280] I. Khan, N. Sun, Z. Zhang, Z. Li, M. Humayun, S. Ali, Y. Qu, L. Jing, Improved visible-light photoactivities of porous LaFeO3 by coupling with nanosized alkaline earth metal oxides and mechanism insight, Catalysis Science & Technology, 9 (2019) 3149-3157.
[281] J. Zhang, Z. Zhu, J. Jiang, H. Li, Fabrication of a novel AgI/LaFeO3/g-C3N4 dual Z-scheme photocatalyst with enhanced photocatalytic performance, Materials Letters, 262 (2020) 127029.
[282] Y. Xu, L. Ding, Z. Wen, M. Zhang, D. Jiang, Y. Guo, C. Ding, K. Wang, Core-shell LaFeO3@g-C3N4 p-n heterostructure with improved photoelectrochemical performance for fabricating streptomycin aptasensor, Applied Surface Science, 511 (2020) 145571.

Muhammad Humayun was born in Charsadda, Pakistan. He obtained his PhD degree in Chemistry & Materials Science from Heilongjiang University China in 2017. From Aug 2017-Dec 2020, he worked as a Postdoc in Prof. Wei Luo group at School of Optical and Electronics Information, Wuhan National Laboratory for Optoelectronics, Huazhong University of Science & Technology (HUST) China. Currently, he is working as a Research Fellow in the same group. He is the author, co-author of more than 50 peer-reviewed publications with citations over 1800. His current research interests include the design of functional photocatalysts & electrocatalysts for energy and environmental applications.

Habib Ullah got his MS in Physical Chemistry in 2014, from the University of Peshawar, Pakistan. He completed his PhD in Renewable Energy from CEMPS, University of Exeter, United Kingdom, in 2018. Currently, he is working as a Research Fellow at the same University. He has published 40 peer-reviewed papers with citations more than 1400. He is also a guest editor of Energies – MDPI. His research involves DFT & Experimental study of *Energy Materials, i.e.,* Conjugated Polymers, Metal Oxides, Perovskite, and Phase Change Materials.

Muhammad Usman received Ph.D. from Chinese Academy of Sciences, P.R China in 2014. After completing two postdoctoral fellowships from Tsinghua-University China and UC-Berkeley Global-Science Institute for four years, he joined Center of Excellence in Nanotechnology, King Fahd University of Petroleum and Minerals, Saudi Arabia as Research Scientist-III (Assistant Professor). His research activities aimed the utilization of Zeolites, Metal-Organic Frameworks (MOFs) and Covalent Organic Frameworks (COFs) for CO_2 capture, separation and conversion. Currently, Muhammad Usman holds seven US patents, published more than 40 peer-reviewed international journals in addition to several conference proceedings/presentations.

Aziz Habibi-Yangjeh received Ph.D. degree in Physical Chemistry from Sharif University of Technology. Now, he is working as a full Professor of Physical Chemistry in University of Mohaghegh Ardabili Iran. His area of research interest mainly includes semiconductor photocatalysis for energy & environmental applications. He has published more than 220 peer-reviewed papers with citations over 10000. He was selected as top 1% scientists in the world by ISI-ESI Thomson Reuters since 2020.

Asif Ali Tahir got his PhD degree from the Department of Inorganic Chemistry, Quaid-i-Azam University, Pakistan, in 2009. He worked as a research associate at Loughborough University for three years and then moved to the University of Liverpool before joining the College of Engineering, Mathematics and Physical Sciences (CEMPS) at the University of Exeter as a Senior Lecturer in Renewable Energy. He specializes in the fabrication of nanomaterials using state-of-the-art techniques for solar energy conversion and photocatalysis. His research focus includes the design, synthesis, and characterization of new materials using soft chemistry approaches and the optimization of nanomaterials for high performance.

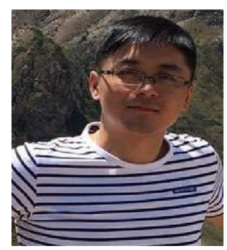

Chundong Wang received his Ph.D degree from City University Hong Kong. Currently, he is working as an Associate Professor at Wuhan National Laboratory for Optoelectronics, Huazhong University of Science and Technology (HUST) Wuhan, China. His research interest includes the design of highly efficient electrocatalysts for energy applications. He is the author, co-author of more than 130 peer-reviewed papers with citations over 4000.

Wei Luo was born in Hubei, China. He received his PhD degree in 2009 from Huazhong University of Science & Technology (HUST) China. From 2009-2012, he worked as a Postdoc in HUST. From 2014-2016, he worked as a Postdoc in the University of Michigan (Ann Arbor). Since 2016, he has been working as an Associate Professor at School of Optical and Electronics Information, Wuhan National Laboratory for Optoelectronics (HUST). His current research interests include the design of SAW sensors, low-dimensional semiconductor sensing materials, and energy materials.